Chapter 4

PLANETARY SURFACES

4.1 The Absence of Bedrock

A striking and obvious observation is that at full Moon, the lunar surface is bright from limb to limb, with only limited darkening toward the edges. Since this effect is not consistent with the intensity of light reflected from a smooth sphere, pre-Apollo observers concluded that the upper surface was porous on a centimeter scale and had the properties of dust. The thickness of the dust layer was a critical question for landing on the surface. The general view was that a layer a few meters thick of rubble and dust from the meteorite bombardment covered the surface. Alternative views called for kilometer thicknesses of fine dust, filling the maria. The unmanned missions, notably Surveyor, resolved questions about the nature and bearing strength of the surface. However, a somewhat surprising feature of the lunar surface was the completeness of the mantle or blanket of debris. Bedrock exposures are extremely rare, the occurrence in the wall of Hadley Rille (Fig. 6.6) being the only one which was observed closely during the Apollo missions. Fragments of rock excavated during meteorite impact are, of course, common, and provided both samples and evidence of competent rock layers at shallow levels in the mare basins.

Freshly exposed surface material (e.g., bright rays from craters such as Tycho) darken with time due mainly to the production of glass during micrometeorite impacts. Since some magnetic anomalies correlate with unusually bright regions, the solar wind bombardment (which is strongly deflected by the magnetic anomalies) may also be responsible for darkening the surface [1]. Infrared and radar mapping from the Earth revealed many "anomalies" or "hot spots" on the lunar surface [2]. The regions around young ray craters show high eclipse temperatures and scatter radar signals strongly. These properties correlate with, and are caused by, the block fields surrounding

young craters. The anomalies fade into the average lunar surface values with increasing age. A corollary is that fracturing and destruction of fresh rock surfaces by impacts must be a common lunar process [2]. On Mars, the mantling effect of wind-deposited fine material likewise hampers direct observations of bedrock, except perhaps at high elevations. The summit calderas of Olympus Mons (Fig. 2.23b) may be an excellent sampling locality, possibly free of regolith or dust. The megaregolith is dealt with in Chapter 5 on planetary crusts (Section 5.1.2).

4.2 The Extreme Upper Surface

Observations are restricted mainly to the lunar surface. Measurement of conductivity indicates that the top layer is strongly insulating [3]. The exposure of lunar soils to humid terrestrial atmospheres causes large changes in the dielectric constant [4]. Curiously, the electrical properties of the surfaces of Mercury, Mars and Venus appear to be very similar to those of the Moon [3, 5]. This is readily understandable for Mercury which lacks an atmosphere and resembles the Moon in many respects. It also appears that water is not affecting the surface electrical properties of Mars, where the temperatures and pressure at the surface are usually below the triple point for water. Local exceptions may be found on Mars where the daytime temperature rises high enough for liquid water to exist on the surface, and local freeze-thaw conditions may exist. The presence of subsurface ice, permafrost and hydrated minerals may change conductivity at deeper levels [6]. On Venus, in contrast, the temperatures and pressures are far above the critical point for water [3] so that on all the inner solar system bodies (except the Earth), liquid water does not affect the electrical properties of the top surface layer.

The temperature on the lunar surface increases by about 47° K in the top 83 cm. The top surface (2–3 cm) is a loosely packed porous layer. Surface temperatures vary considerably. At the Apollo 17 site, the surface reaches a maximum of 384° K (111° C) and cools to 102° K (–171° C) at the end of the lunar night [2]. The near-surface temperature is 216° K (–57° C). At the Apollo 15 site, these temperatures are about 10° K lower. The agreement with previous estimates based on terrestrial observations was very close [8, 9].

The temperature range at the Viking sites on Mars was between 150° K (–123° C) and 240° K (–33° C) [7]; Mercury temperatures range from 93° K (–180° C) to 700° K (430° C) and surface temperatures on Venus are about 720° K (450° C).

The question of the lateral movement of the surface layer or of underlying layers has been extensively discussed (e.g., [10]). Although much material has been redistributed by impact processes (e.g., Figs. 2.1, 2.14), the underlying bedrock is the dominant influence on the composition of the regolith. The

truth of this statement is apparent from the chemistry of the soils at the various sites, with minor exceptions [11]. The chemical data from the orbital experiments (Al/Si, Mg/Si, and the gamma-ray Th values) show breaks generally coincident with the mare-highland boundaries [12]. Thus, movement of a surficial layer occurs only on a local scale, and the chemistry and nature of the regolith is dominated by local bedrock components.

Evidence for local stirring of the very top dust layer has been deduced from the light scattering observed at the terminator by the Apollo 17 astronauts [13]. These observations are consistent with effects observed by Surveyor 6 and Lunokhod 2, and are perhaps due to dust levitation caused by temperature changes at the terminator [13, 14]. The effect does not produce any widespread migration of dust, which would blur the sharp mare-highland boundaries observed by the orbital chemical analyses [12]. Chemical and isotopic processes occurring in the upper layer of the regolith are discussed further throughout this chapter.

The importance of the very top layer in cosmic ray, solar flare, and track studies has led to the development of new sampling techniques. One such device consists of a free-floating cloth-covered plate designed to sample the top 100 micron layer. Another, a spring-loaded cloth-covered plate, sampled the top 0.5 mm [15]. Other samples in this category, from the Apollo 16 highland site at Descartes, include top and bottom samples from a boulder and soil samples from shadowed areas. Work on this material is still in progress.

Direct stereo photography with 80 micron resolution at the surface was carried out by the astronauts on the Apollo 11, 12 and 14 missions [16]. The astronauts' comments that the upper surface resembled a beach following a heavy rain shower were interpreted as the effect of micrometeorite bombardment.

4.3 The Regolith

The regolith is the continuous layer, usually several meters in thickness, which covers the entire lunar surface [17]. It is a debris blanket in every sense of the term, ranging from very fine dust to blocks several meters across (Fig. 4.1). Although the finer components (< 1 mm) are often referred to as soil, the distinction from terrestrial soils, formed by the complex interaction of the atmosphere and biosphere on rocks, is complete. The active processes on the Moon at present are cosmic, not planetary. Bombardment of the surface occurs at all scales from impacts which produce craters such as Tycho and Copernicus to erosion by particles producing sub-micron-sized pits, while cosmic ray and solar flare particles produce effects on an atomic scale. The surficial material is saturated with solar wind gases.

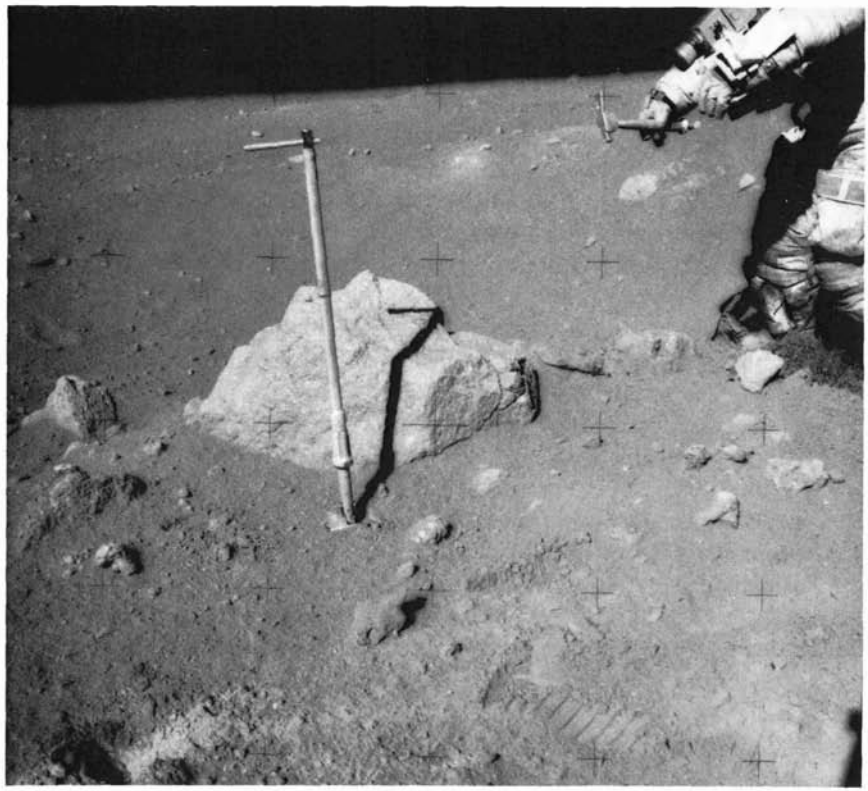

4.1 The regolith at Station 8, 3.4 km northeast of South Ray crater (Apollo 16 site). The boulder is the source of gabbroic anorthosite samples 68415 and 68416 (NASA AS-16-108 17697).

4.3.1 Thickness and Mechanical Properties

The thickness of the regolith has been established mainly by observations of those craters that are seen to excavate bedrock, and by direct observations along the edge of Hadley Rille [18]. Here, the base is seen to be irregular. The average thickness of the regolith on the maria is 4–5 m, while the highland regolith is about twice as thick (averaging about 10 m), due both to a longer exposure history and to a more intense meteorite flux.

The regolith, although quite variable locally in thickness, has very similar seismic characteristics at all sites (highlands and maria alike), typically with very low seismic velocities of about 100 m/sec [19] (Fig. 4.2). The value ranges over the different Apollo sites (Apollo 12–17) from 92–114 m/sec, indicating that the processes producing the regolith formed material of uni-

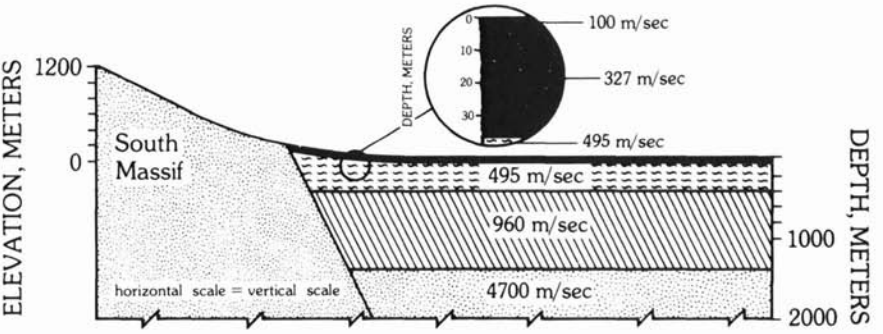

4.2 A cross-section of the regional structure at the Apollo 11 landing site in the Taurus-Littrow valley [19].

form seismic properties moon-wide from different mare and highland source materials. The seismic velocities increase rapidly below the regolith. At the Apollo 17 site the velocity reaches 4.7 km/sec. at a depth of 1.4 km. That is good evidence that the subsurface material is not dust but basaltic flows, fractured near the surface and underlying a few meters of regolith. This conclusion is strengthened by the orbital radar evidence for basin-wide subsurface reflectors at depths of 0.9 and 1.6 km in Mare Serenitatis, and at 1.4 km in Mare Crisium [20].

There are many local variations in regolith thickness. Perhaps the most extreme example is in the Taurus-Littrow Valley where, near the landing site, thickness ranged from 6.2 to 36.9 m. It can be argued that such changes are due to the local concentration of medium-sized craters (such as Camelot, 700 m in diameter) producing uneven thicknesses due to local throwout, burying smaller craters.

Regolith thicknesses on the Cayley Plains at the Apollo 16 site vary between 6 and 10 m, but may be up to 20 m on the Descartes Mountains [21]. Regolith development on the rims of young craters is very limited. The thickness on the rim of North Ray crater (Apollo 16 site) is only a few centimeters. North Ray crater is 50 million years old [22] (Fig. 4.3).

The bulk density of the soils ranges from 0.9 to 1.1 g/cm^3 at the top surface, but increases with depth to values up to 1.9 g/cm^3. The density increases markedly in the upper 10–20 cm [23, 24]. The porosity of the upper surface is 45%, with higher values around crater rims, as judged from soil mechanics studies of the astronauts' footprints. Thus, the top surface is very loose, due to stirring by micrometeorites, but the lower depths, below about 20 cm, are strongly compacted, presumably by shaking during impacts. The compressibility of the soil is similar to that of ground-up terrestrial basalt.

4.3 North Ray crater, 900 m in diameter, viewed from Station 11 at the Apollo 16 Descartes site. The regolith on the rim of this 50-m.y.-old crater is only a few centimeters thick (NASA AS-16-116 18599).

All of these mechanical properties, vital for manned landings and astronaut surface activities, have been extensively studied [23, 24]. Notwithstanding the differences in composition, particle size and shape, and grain size distribution, from a soil mechanics or engineering point of view the lunar soil does not differ significantly in its behavior from what would be expected on Earth of granular, slightly cohesive terrestrial soil with the same particle size distribution and packing characteristics. The one major difference that might be singled out is the interparticle adhesion of lunar soil, which is demonstrated, for example, by the sharp vertical walls produced by the indentation of the footprints and by the difficulty of handling lunar powders in the laboratory.

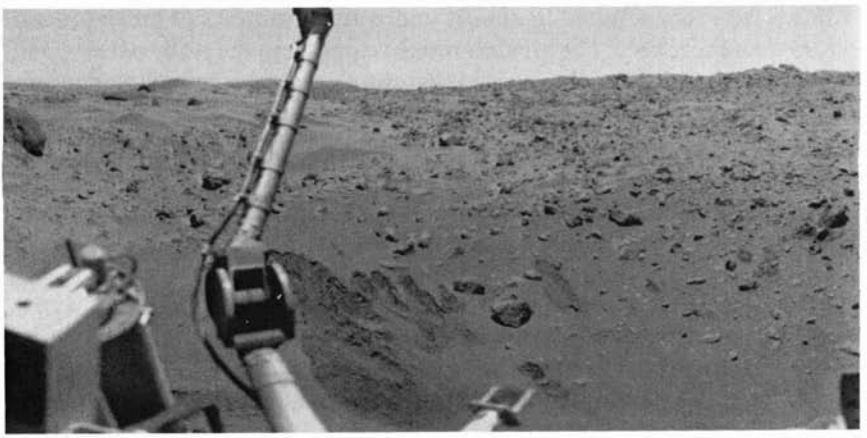

4.4 View of the Martian surface from the Viking 1 lander in Chryse Planitia.

The similarity of lunar soil in mechanical properties to those of terrestrial examples is due to the fact that the mechanical properties depend on size, density, and shape of the particles rather than on their chemical composition. The consensus from the soil mechanics studies [24] and from the seismic data [19] is that the mechanical properties of the lunar soils are about the same at all sites. With the exception of two photographs of the Venusian surface, Mars is the only other body in the solar system for which we have some detailed knowledge of the nature and properties of its surface (Fig. 4.4). The clarity of the photographs enables unambiguous interpretations to be made. The surface layer appears to be firmer than that of the lunar regolith [7]. The fine-grained material is strongly adhesive, like the lunar fines. Bulk density is about 1.2 gm/cm^3. Small weakly cohesive clods are common and the soil contains many more large rocks than the lunar regolith. The presence of dunes indicates substantial wind transport and fine material will thus be selectively removed. Remote sampling of such material would not yield the fragments of rocks commonly found in the lunar soils.

4.3.2 Structure

The layered nature of the regolith has now been revealed by many core samples. A total of 26 core samples of varying depths up to 3 m were taken during the missions, along with many scoop samples of soil. The cores provided valuable data after some initial confusion due to the early sampling techniques, which did not return undisturbed cores. The deepest core (294.5 cm) was at Apollo 17. Core tube samples from Apollo 11, 12, and 14 missions produced disturbed samples, but on Apollo 15, 16, and 17 missions, use of

thin-walled tubes resulted in almost undisturbed samples of lunar soil with 90–95% core recovery. The greatest insight came from the study of the Apollo 15 deep core, which clearly revealed that the regolith was not a homogeneous pile of rubble. Rather, it is a layered succession of ejecta blankets. An apparent paradox is that the regolith is both well mixed on a small scale and also displays a layered structure. For example, the Apollo 15 deep core tube, 242 cm long, contained 42 major textural units ranging from a few millimeters to 13 cm in thickness. There is no correlation between layers in adjacent core tubes and the individual layers are well mixed.

This paradox is resolved as follows. The regolith is continuously gardened by meteorites and micrometeorites. Each impact inverts the microstratigraphy and produces layers of ejecta, some new and some containing remnants of older layers. The new surface layers are stirred by micrometeorites.

A complex layered regolith is thus built up, but is in a continual state of flux. Particles now at the surface may be buried deeply by future impacts. In this manner, regolith is turned over like a heavily bombarded battlefield. The layering in a core tube has no wider stratigraphic significance. It is local and temporary. The result is that we have the well-stirred and homogeneous regolith, with one portion very like another, uniform moon-wide, as shown by the seismic data, yet layered locally.

These processes have been placed on a quantitative basis [25, 26]. The most important result is that the turnover rate of the regolith decreases rapidly with depth. "While it takes approximately 10^7 yr. to excavate the regolith at least once (with 99% probability) to a depth of 9 mm, it will take 10^9 yr. to excavate to a depth of 7 cm; simultaneously, however, the uppermost millimeters of the regolith has [sic] been turned over approximately 700 times in 10^7 yr. and many thousands of times in 10^9 yr." [26, p. 9].

The upper one millimeter of the regolith is the zone where most reworking and mixing by micrometeorites occurs on these models. There is some indication from measurements of cosmogenic radionuclides that these depth estimates may be too low. Thus, studies employing ^{53}Mn (half-life of 3.7 million years) on the Apollo core samples [27] indicate a mean depth of disturbance, over 10^7 yr. to be about 5–6 g/cm^2 (about 3 cm). The difference between these two estimates depends partly on the mass distribution of the impacting bodies, but also indicates the difficulties in modelling these processes.

The calculations with respect to vertical mixing within the regolith, discussed above, are much more readily treated than are the problems of local and exotic components in the regolith at a particular landing site. Lateral transport is not particularly efficient; otherwise, the regolith would be laterally homogeneous over broad areas. This lack of homogeneity is reflected in the fact that the admixture of mare and highland soils close to geological boundaries is surprisingly small. Mare-highland contacts appear relatively

sharp on orbital geochemical data. At the Apollo 15 and 17 sites, steep chemical and petrological gradients in soil compositions occur over distances of a few kilometers. According to early calculations, about five percent of the regolith at a site may be derived from distances greater than 100 km, while 0.5 percent come from distances greater than 1000 km. Fifty percent comes from distances less than 3 km [28–30]. Thus, most of the regolith is of local origin. In accordance with the predictions, components of the Apollo 11 soil sample were derived from highland sources, leading to the identification of the highlands as "anorthositic" [31]. However, Hörz [26, p.11] has drawn attention to the apparent anomaly that most genuine mare soils (e.g., Apollo 11, 12 and Luna 16) contain 10–30% of non-mare material, and that this is constant over wide areas of mare soils, increasing only within 5 km of exposed highlands. A current problem is whether such material is derived from highland material at shallow depths beneath the mare basalts.

4.3.3 Rate of Accumulation

The accumulation rate for the past three aeons of the lunar regolith averages about 1.5 m per aeon [32], 1.5 mm per million years, or about 15 angstrom units per year corresponding to a layer of about 6 oxygen anions. However, such averages are misleading. The accumulation of the regolith occurs as a result of the addition of discrete layers, and is not continuous. The local accretion rate is extremely variable. In comparison with terrestrial erosion and deposition, lunar processes are slow indeed.

The accumulation rate, which is directly related to the meteoritic cratering flux (Section 3.16), steepens appreciably in the period between 3.5 and 4 aeons. The present regolith in the highlands dates from about 3.8 to 4.0 aeons, which marked the close of the intense bombardment, culminating in the impacts that formed the Imbrium and Orientale ringed basins. The accumulation rate for the period 3.5–4.0 aeons is about an order of magnitude greater than in younger epochs. A complicating factor is that the regolith does not grow at a constant rate, even if the meteorite flux is steady [25]. As the regolith increases in thickness, it buffers the bedrock against the smaller impacts. Larger impact events are thus required to generate fresh bedrock debris. With increasing regolith thickness, samples from deeper source areas will be added to the top surface [25].

4.3.4 "Ages" of the Soils

The exceedingly complex mixture represented by the soil contains components of varying ages. This was dramatically emphasized by the apparent paradox from initial investigations that the mare soils had model Rb-Sr ages around 4.6 aeons, although they were lying on and principally derived from

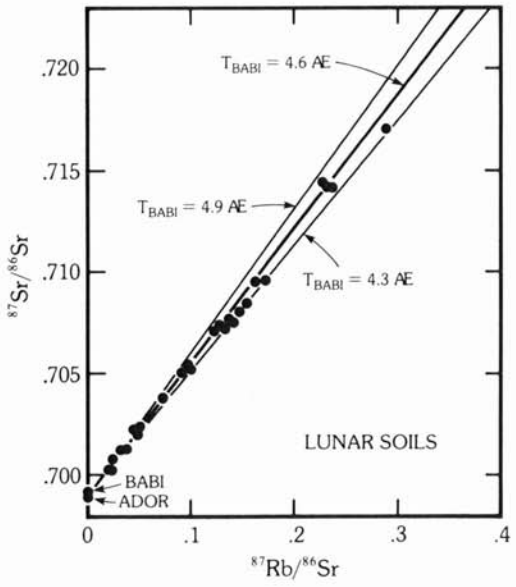

4.5a Rubidium-strontium evolution diagram for lunar soils. The data are without direct age significance since the soils are complex mixtures. The lines T BABI = 4.3 AE, 4.6 AE, and 4.9 AE show the growth of radiogenic strontium as a function of ^{87}Rb from an inital ratio of 0.69898. This is the Basaltic Achondrite Best Initial ratio or BABI. ADOR is the initial ratio for the meteorite Angros dos Reis and is one of the most primitive ratios known. The initial isotopic ratio $^{87}Sr/^{86}Sr$ for the Moon appears to be close to BABI. Note that using this ratio, the lunar soil data cluster about the 4.6 aeon line [33]. (Courtesy G. J. Wasserburg.)

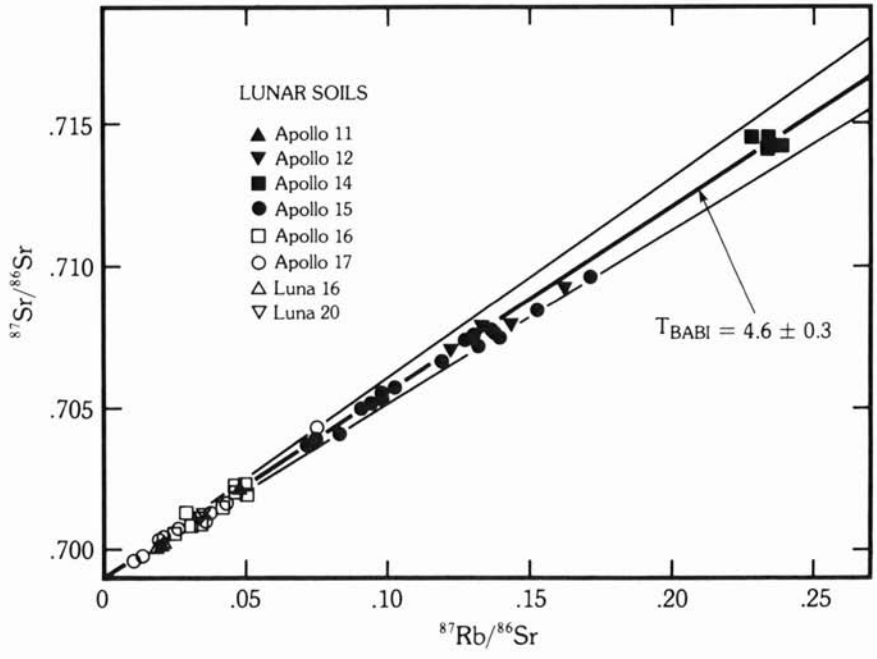

4.5b Rb-Sr evolution diagram for lunar soils. (Courtesy L. E. Nyquist.)

rocks whose crystallization ages, from mineral isochron studies and $^{40}Ar/^{39}Ar$ data, were 3.6–3.8 aeons [33–35]. This effect is shown in Figs. 4.5a and b where soil age data are shown on a conventional Rb-Sr diagram. There is a strong tendency for the soil data to scatter about a line indicating an age of 4.6 aeons, since the material had an initial $^{87}Sr/^{86}Sr$ ratio of 0.69898, equivalent to that observed in basaltic achondrites [36]. These model ages from the soils indicate that the principal fractionation of Rb from Sr occurred at about 4.6 aeons and that the amount of fractionation during partial melting to produce the mare basalts was smaller.

Experience from later missions showed that some soils had model ages greater than 4.6 aeons (Fig. 4.6a and b). There is so much evidence indicating formation of the Moon and the rest of the solar system at about 4.6 aeons ago

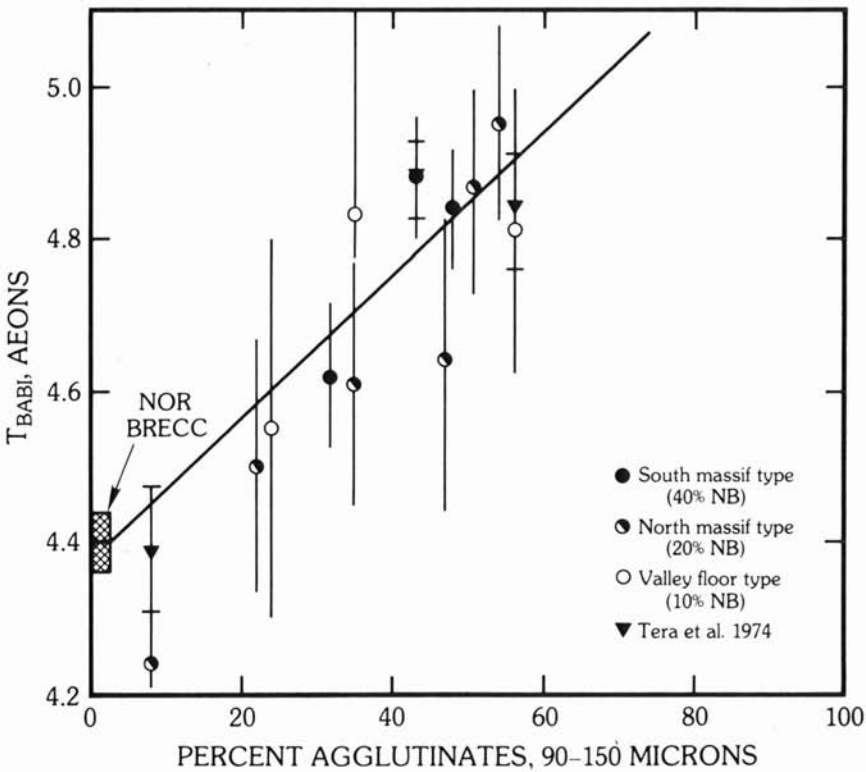

4.6a Model ages for soils as a function of agglutinate content of the soils. As the agglutinate (fused glassy particles) content increases, so does the apparent age of the soils. T BABI is the age (in aeons) based on an initial $^{87}Sr/^{86}Sr$ of 0.69898. NOR BRECC is noritic breccia. The amount of fused glassy particles in the soils is a direct index of the amount of micrometeorite bombardment and hence of soil maturity. (Courtesy L. E. Nyquist.)

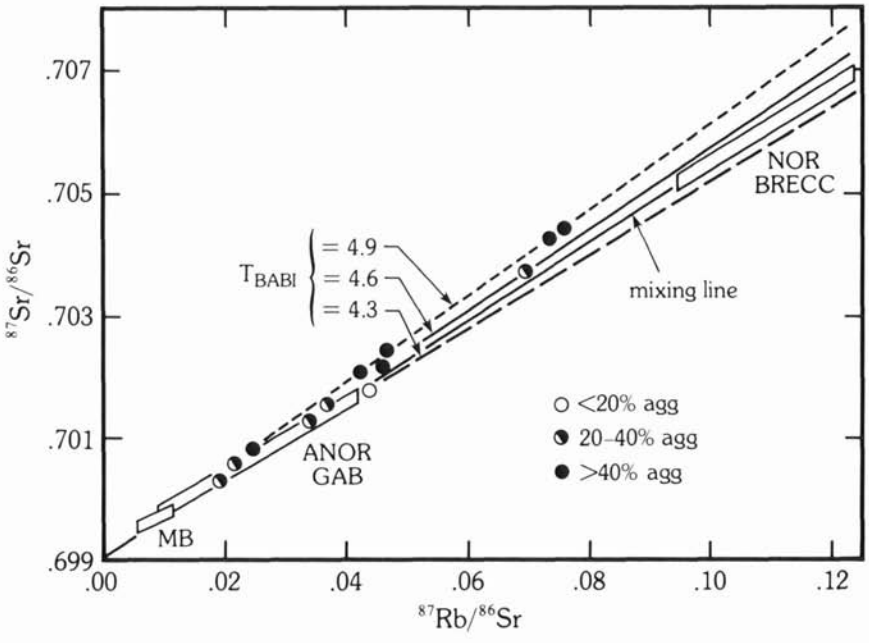

4.6b Rb-Sr evolution diagram for Apollo 17 soils, showing that the apparent age increases with increase in agglutinate (agg) content. MB = mare basalt. ANOR GAB = anorthositic gabbro. (Courtesy L. E. Nyquist.)

(Section 9.2), that apparent ages older than this value indicate that alternative explanations for the data are required. It should be emphasized that there are "no known rock types which can be added to the soils to produce high model ages greater than 4.6 aeons" [37]. This fact strongly argues against explanations that the exotic component is merely a finely divided KREEP component disseminated over the Moon.

Since the soils have arisen by meteorite impact processes repeated many times, it is perhaps not surprising that the delicate interrelationships between radiogenic ^{87}Rb and its daughter product ^{87}Sr might be disturbed occasionally. Thus, small losses of volatile Rb relative to Sr during melting and glass formation at elevated temperatures provide a way to produce old apparent ages [37] as is shown by the correlation between age and agglutinate formation.

These problems with age dating of the lunar soils provide a salutary lesson, not appreciated before the Apollo missions. This dearly bought experience enables us to obtain meaningful ages from clasts separated from soils as was amply demonstrated by the analysis of fragments from Luna 16, 20 and 24 samples. This lesson will be a valuable one in future sampling missions.

4.3.5 Soil Breccias and Shock Metamorphism of Lunar Soils

Soil breccias, consisting of weakly indurated mixtures of rock fragments (Fig. 4.7), glass and fine soil, achieved an undue early prominence by comprising about half of the initial Apollo 11 sample return. Experimental work has shown that single meteorite impacts into soil can produce these breccias [38]. Using a 20 mm powder gun to simulate shock pressures between 150 and 730 kbars, the lunar soil was compacted and partially remelted to form agglutinates and soil breccias. *In situ* melts of agglutinates and melts along grain edges occur at low pressures. The highest pressure shock melts are closest in composition to the bulk soil composition. Propagation of shock waves from a single impact in soils causes collapse and shear of grains, collapse of pore spaces, and compaction which indurates the soil at low pressures (150–180 kbars) with less than 5% melting. These resemble soil breccias. As the pressure increases, the amount of intergranular melt and shock melting increases. Above 650 kbars, 30–75% of the sample melts, producing a pumiceous glass. Thus, the formation of soil breccias does not require sintering in hot base surge deposits [39] or repetitive impacts [40].

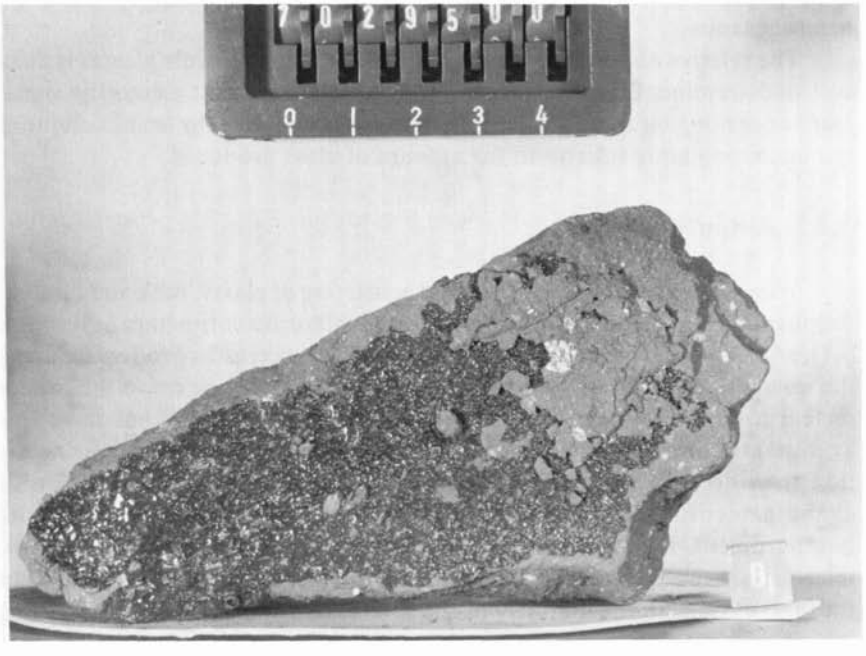

4.7 Soil breccia 70295 showing glass coating (NASA S-73-17192).

4.4 Glasses

Many varieties of glasses are found in the lunar soils. The existence of the glasses is mostly due to melting during meteorite impact, but some important exceptions occur. The emerald green glass from Apollo 15 provides us with a primitive basaltic composition. The orange glasses from Taurus-Littrow (Apollo 17) contribute to our knowledge of the dark mantle and of the mechanism of mare basalt eruption. These and other glasses of possible volcanic origin are discussed in Chapter 6 on basaltic volcanism (Section 6.2.3). The emphasis here is on the common and abundant impact-derived glasses.

Because the more spherical varieties of the glasses are abundant and generally homogeneous, they are suited to chemical analysis by electron microprobe techniques. This enables estimates to be made of the frequency of various chemical compositions, which may then be related to the parental rocks. This approach is important for the heavily cratered and brecciated highlands, where terrestrial petrographic experience and techniques have been less readily adapted to lunar studies than was the case with the mare basalts. However, in these studies, care must be taken to avoid bias and the identification of mixtures as primary rock types. There are many non-homogeneous glasses, while the agglutinates (Section 4.4.1) are particularly heterogeneous.

The relative abundance of impact-produced and volcanic glasses is difficult to determine. Even the absence of siderophile element meteoritic signatures does not guarantee a volcanic origin, on account of the small volume of the impacting body relative to the amount of glass produced.

4.4.1 Agglutinates

These are glass-bonded aggregates consisting of glassy, rock and mineral fragments (Figs. 4.8, 4.9). They form during micrometeorite impact into soil [41], and may be in part the remnants of small glassy craters produced during the impacts. Their abundance in a soil is an index of exposure to the micrometeorite bombardment and hence of soil maturity. Soils that have low agglutinate contents contain evidence of a shorter exposure to cosmic radiation than do soils with a high agglutinate content [42]. The formation of agglutinates offsets the grinding up of the soil particles by the micrometeorite bombardment. Eventually an equilibrium grain size in the soils of about 60 microns is reached by these two competing processes. The agglutinate content thus increases with the maturity of the soil.

In general, the average composition of the glassy portion of agglutinates is that of the soil in which they were formed, providing the soil is mature. Accordingly, such compositions may be used in complex regoliths to deter-

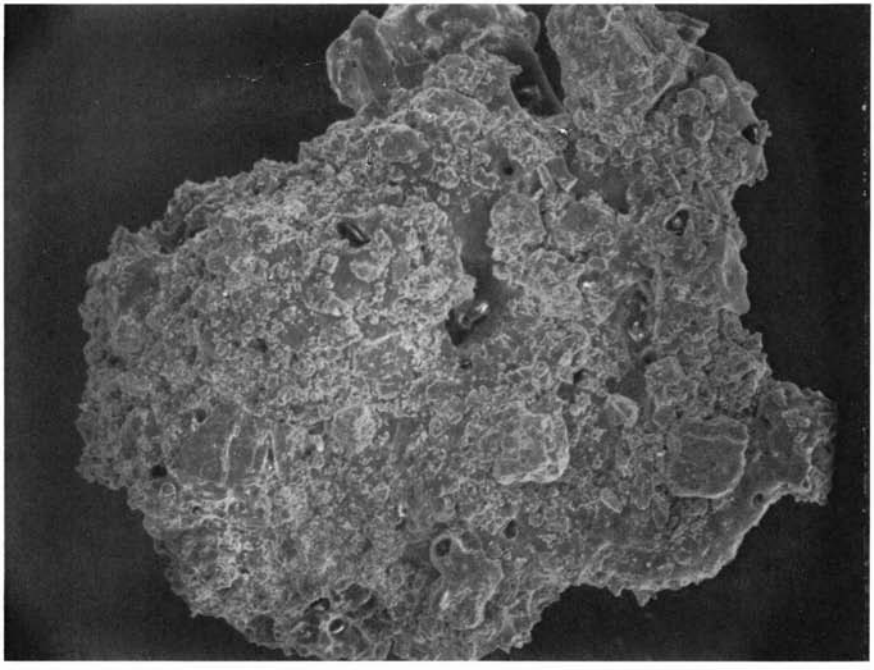

4.8 SEM photo of an Apollo 12 agglutinate, consisting of lithic, mineral and glassy debris bonded together by inhomogeneous glass. Width of photo is 1 mm. (NASA S.70 34983. Courtesy D. S. McKay.)

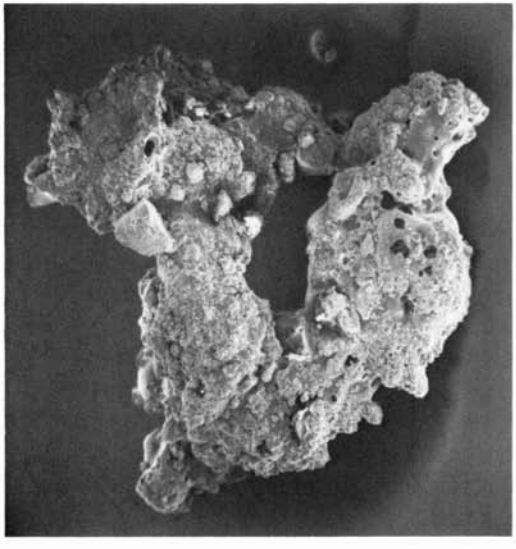

4.9 SEM photo of a 1-mm Apollo 12 agglutinate particle. (NASA S71-24575. Courtesy D. S. McKay.)

mine fossil soil compositions. For example, at the Apollo 17 site, it is possible to calculate the contribution to the regolith from the landslide at the South Massif. Pre-Camelot crater soils and pre-central cluster soils can also be identified by this approach [43]. These considerations place some restrictions on mixing calculations for soils. It is clear that such chemical calculations should always be accompanied by petrographic examination of the soils, particularly in areas such as the Apollo 17 regolith where agglutinates formed from mature soil compositions may be mixed with freshly excavated material [43].

For some time, it was thought that major elemental fractionations occurred during the formation of agglutinates [44]. Detailed analysis of agglutinate fractions separated by magnetic separation techniques showed increases in the concentration of the ferromagnesian elements (Fe, Mg, Ti) and decreases in the abundances of Na, Ca, Al and Eu, typical constituents of plagioclase. These effects were attributed to selective melting of pyroxene during agglutinate formation, relative to the more refractory plagioclase. However, like other impact-produced partial melting scenarios on the Moon, this effect is not real. The magnetic separation processes used to separate the agglutinate fractions were biased not only toward magnetic agglutinates, but also select magnetic non-agglutinates (e.g., pyroxenes, ilmenites and olivines with included Fe-Ni grains). The non-magnetic residue was selectively enriched in non-magnetic agglutinates, including plagioclase compositions. Accordingly, the proposed chemical fractionations were an artifact [45]. It has been proposed that agglutinates form by preferential fusion of the finest (<10 micron) fraction of the soils [46] but this model requires much testing before it can be substantiated.

4.4.2 Impact Glasses

Many different forms have been described. The spheres are typically about 100 microns in diameter, but range widely in size. Ellipsoidal shapes, dumbbells, teardrops, and rods, are common (Figs. 4.10, 4.11). These are the typical rotational shapes assumed by splashed liquids. Some of the spheroidal forms are flattened, indicating that they were plastic when they landed. There is a great abundance of angular fragments. Many of these are broken pieces of the more regular forms. Others occur as large irregular masses (>10 g) coating rocks or as linings in pits clearly produced by impact of small particles. The outer surfaces of the spherules commonly have small craters.

A wide range in color is shown by the glasses from colorless through pale yellow, green, brown, orange to red, and black. The colors show a clear relation to refractive index and to composition. Table 4.1 shows the interrelationship of color, refractive index and density. (See also Section 6.2.3 on the emerald green and orange glasses.) The color of the glasses is clearly reflected

4.10 Ropy glass fragment, 1 mm long, of KREEP glass (12033). (NASA S.70 17107. Courtesy D. S. McKay.)

in the chemistry. The lighter colored glasses are similar in composition to the feldspathic or anorthositic fragments, whereas the more numerous red, yellow and dark brown glasses resemble the bulk analyses of the rocks and the fine material.

Tiny spherules of iron are present in many of the glasses. They are normally less than 30 microns in diameter and are especially frequent in the heterogeneous glasses. Some of these spherules contain about 10% Ni as well as troilite and schreibersite, which are common minerals of iron meteorites.

Others, probably the majority, are derived by auto-reduction of Fe^{2+} (see Section 4.5.1). These contain nickel-free iron and troilite derived from the lunar rocks, forming immiscible droplets in the glass melt. The chief evidence for an external meteoritic origin for the nickel-rich iron spheres is their nickel content, since nickel is very depleted in the parental rocks. These nickel-iron spheres resemble those found in terrestrial glasses that have been formed at meteorite craters by the fusion of country rock by the impacting iron-nickel meteorite. The presence of these globules indicates that most of the glasses

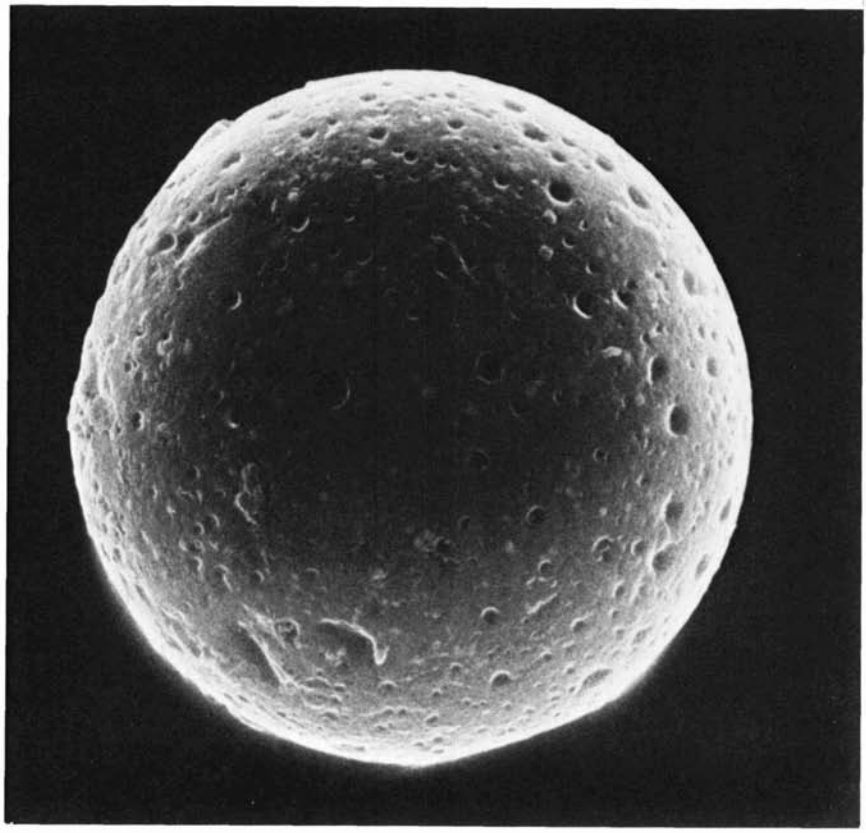

4.11 SEM photo of Luna 24 glass sphere, showing some superficial resemblance to Tethys. The pits are due to removal of included iron spherules, and not to impact. (NASA S.78-36991. Courtesy D. S. McKay.)

Table 4.1 Relationships between color and other properties of lunar glasses.[†]

Color	Refractive Index	TiO_2 (%)	FeO (%)	Density
Colorless, transparent	1.50–1.60	0–0.1	0–1.6	< 2.7
Light yellow, green to light green, transparent	1.59–1.65	0.1–2	4–10	2.7–2.8
Dark green, transparent	1.65	0–1	7–16	2.8–2.9
Yellow-brown, transparent	1.65	1–2.5	8–14	2.7–2.8
Light to dark brown and red-brown, transparent	1.65–1.75	3–8	9–16	2.8–3.0
Dark brown to opaque	1.75	7–12	15–25	3.0–3.25

[†]From Frondel, C. (1970) *PLC 1:* 450.

bear a genetic relationship to meteorite impact. Most of the surface features, such as small craters, pits, splashes of glass (Figs. 4.12a and b) and iron beads are the result of meteorite impact. There are no major differences in chemical composition between the angular glass fragments and the spheroidal forms.

The range in composition found among the glasses can be due to several causes:

(a) Melting of whole rocks and bulk samples of fine material, giving the range in composition found for the rocks.

(b) Melting of individual mineral phases by impact of small particles.

(c) Selective vaporization. The overall evidence seems to indicate that this process was not effective in altering the composition to any marked degree. Studies from terrestrial glasses support this contention. Thus, at the Lonar Crater, India, the glasses are identical in composition to the parental basalts [47] supporting similar conclusions for impacts into terrestrial sedimentary rocks [48]. Evidence of rather thorough mixing to produce homogeneous glasses from diverse target rocks occurs at large terrestrial impact sites, such as Manicouagan [49]. This question becomes important in studying the highland samples, where most of the evidence for primary rocks has to be inferred.

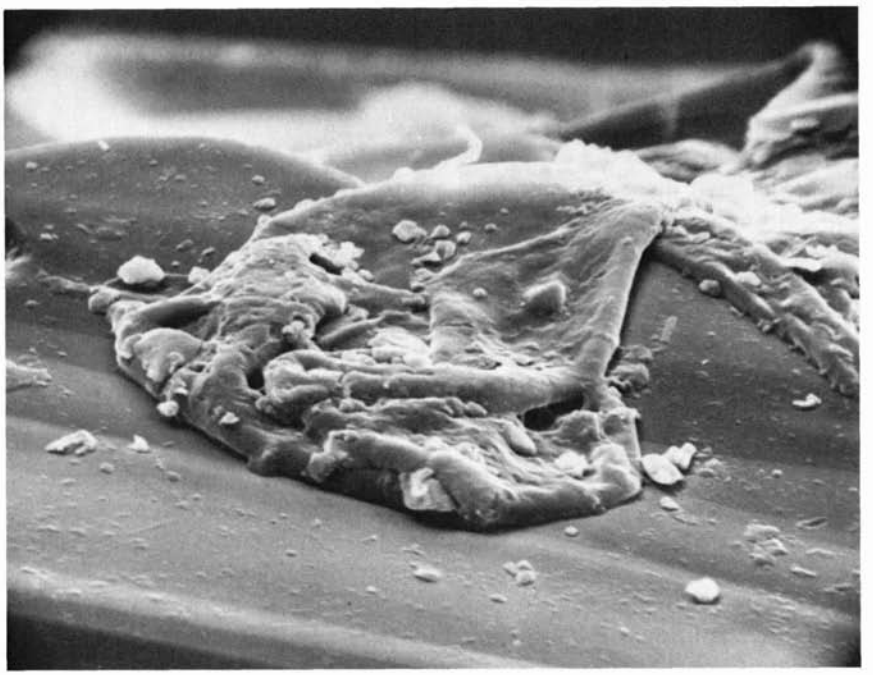

4.12a Glass splash on a lunar olivine crystal. The width of the "lava flow" is 100 microns. (NASA S.71 24637. Courtesy D. S. McKay.)

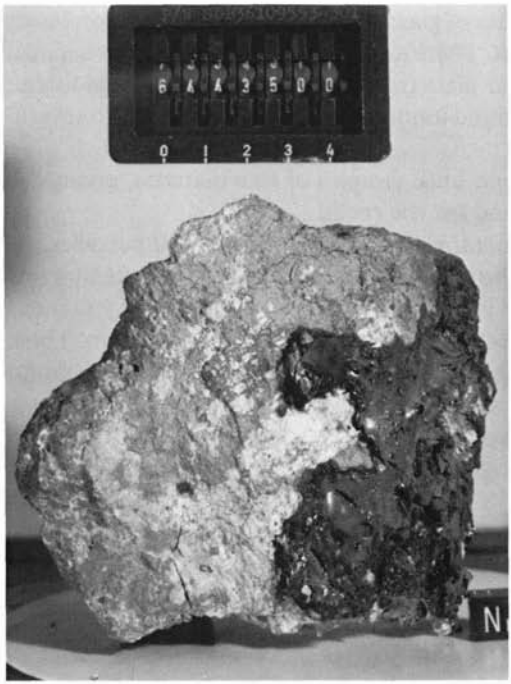

4.12b Glass coating Apollo 16 lunar breccia 64435 (NASA S.72-39674).

(d) Selective melting of specific minerals; e.g., under shock conditions, feldspar melts at lower pressures than does pyroxene or olivine.

Although there are some similarities in form between the spherules and chondrules observed in chondritic meteorites, detailed textural studies of chondrules [50, 51] do not provide many direct analogies, and do not directly support an origin for chondrules in a lunar-type regolith. The chondritic meteorites are, of course, different in composition from the lunar breccias, and there is ample evidence from the Apollo studies that the chondritic meteorites are not derived from the Moon.

A final observation concerning the resemblance between some glass forms and microfossils deserves wide circulation: "The abundant spheroids and ovoids are similar in shape to some algal and bacterial unicells, and the smaller ones are comparable in size. Indeed, if such particles were coated with carbon, they would make impressive pseudomicrofossils . . . .This is not to propose that there are or were solid glass Protozoa on the Moon, but to add one more warning about a too-ready interpretation of exotic objects as of vital origin on the basis of gross morphology alone . . . . This warning deserves emphasis. Elsewhere on the lunar or Martian surface may be lifelike artifacts that will be harder to discriminate from the real thing" [52].

4.4.3 Tektites

One of the achievements of the Apollo missions was to solve the long-standing scientific question of a terrestrial versus lunar origin for tektites [53]. Before Apollo 11, it was the scientific consensus that tektites were melted and splashed material formed during large cometary or meteorite impact events. Whether the impact took place on the Earth or the Moon was the topic of an intense scientific debate. These impact events were large-scale since the tektites were sprayed over immense distances. In the Australian strewn field, tektites occur across the entire southern half of the continent. The numerous occurrences in Southeast Asia are related to the same event, and the occurrence of microtektites in deep-sea cores (within the zone marking the 700,000-year reversal of the Earth's magnetic field: Bruhnes-Matuyama reversal) has extended the strewn field to over 4% of the Earth's surface.

Four separate tektite-strewn fields are known: bediasites (North America, 34 million years); moldavites (Czechoslovakia, 14 million years); Ivory Coast (1.3 million years); and Southeast Asian and Australian fields (0.7 million years). No normal geological processes (e.g., volcanic action) are capable of explaining this distribution. Neither do these small objects come from deep space, for they record no evidence of any exposure to cosmic radiation. These facts have restricted their origin to the Earth or the Moon.

Of immediate interest to the tektite problem was the glass present in the lunar soil. Although generally small, these forms resemble the primary tektite forms. The lunar glass, terrestrial volcanic glass, and protected tektite surfaces all show similar features, such as bubble pits, domal gas blisters, abraded and ablated surfaces, and spatter. These features are evidence for similar formational processes, but the consensus among workers on the lunar glasses is that they do not resemble tektites in refractive index, chemistry or infrared spectral characteristics.

The chemistry of tektites reflects that of the parent material (Table 4.2), and losses during formation appear to be restricted to elements and compounds more volatile than cesium. Terrestrial impact glasses provide small-scale analogues of tektite-forming events [48] and indicate that only the most volatile components are lost during fusion. The present composition of tektites can accordingly be used to infer the composition of the parent material.

Tektite chemistry is totally different from that observed in lunar mare basalts. These possess Cr contents that are two orders of magnitude higher than tektites, distinctive REE patterns with large Eu depletions, high Fe and low SiO_2 contents, low K / U ratios, and many other diagnostic features, which are not observed in the chemistry of tektites.

Typical highland compositions with high-Al and Ca and low K concentrations are distinct from those of tektites. Lunar samples with characteristic KREEP-type chemistry have contents of U and Th similar to tektites. How-

Table 4.2 Comparison of lunar and tektite major element compositions.†

	Average Lunar Highlands (1)	Lunar high–SiO_2 glasses (2)	(3)	Bediasite (4)	Moldavite (5)	Indochinite (6)	Javanite (7)	Australite (8)	Bottle-green micro-tektite (9)
SiO_2	44.9	75.8	77.0	73.5	80.7	72.7	73.2	73.8	50.5
TiO_2	0.60	0.53	0.5	0.87	0.32	0.78	0.64	0.67	0.86
Al_2O_3	24.6	11.4	12.0	15.9	9.6	13.6	11.2	11.4	16.7
FeO	6.6	2.5	0.5	5.0	1.93	4.60	5.70	4.31	4.53
MgO	7.0	0.25	0.10	1.38	1.59	2.14	3.75	1.92	20.7
CaO	15.8	1.8	0.5	0.06	2.13	1.98	2.10	3.99	4.81
Na_2O	0.45	0.35	1.0	1.30	0.37	1.05	0.98	1.23	0.05
K_2O	0.11	6.4	8.0	1.73	3.60	2.62	2.09	2.28	0.04
Σ	100.0	99.0	99.6	99.7	100.2	99.5	99.7	99.6	98.2
K_2O/MgO	0.016	25.6	80	1.25	2.3	1.22	0.56	1.19	0.002

† Data in wt.%

1. From Table 5.6.
2. Apollo 11, Roedder, E., and Weiblen, P. W. (1971) *PLC 2:* 522.
3. Apollo 14, Glass, B. P. (1977) NASA Report NGR 08-001-029.

4–5. Baker, G. (1959) Mem. Nat. Mus. Vic. 23.

6–8. Taylor, S. R., and McLennan, S. M. (1979) *GCA.* 43: 1551.

9. Frey, F -A. (1977) *EPSL.* 35: 45.

ever, they retain the lunar characteristics of high Cr and Eu depletion.

Three minor lunar occurrences analogous in composition to K-rich terrestrial granites are (a) late-state glassy K-rich mesostasis found in lunar basalts; (b) immiscible globules of granitic composition; and (c) minor amounts of granitic glasses in lunar soil. All these compositions are typified by high potassium values, typically 6–8%. The Mg contents are very low. None of these compositions resembles those of tektites, which in any event are not closely related to terrestrial granites. In a study of 500 glass particles from lunar soils, Glass [55] found only one spherule with > 60% SiO_2 (62%SiO_2, 4%K_2O), illustrating the rarity of such compositions on the Moon. Evidence for a lunar origin of tektites has been adduced from studies of lunar liquid immiscibility by Roedder and Weiblen [54], who concluded that "any such surface mass (of granitic composition derived from liquid immiscibility) would also remove one of the obstacles to a possible lunar origin for tektites." However, the data do not encourage this speculation. A comparison of K/Mg and K/Na ratios for australites, with the microscopic lunar granitic material, shows that the potash granites have ratios a order of magnitude higher than tektites, while the high silica glasses have ratios 30 to 50 times those of tektites.

The water content of tektites, although low (~80 ppm) is nevertheless at least four orders of magnitude higher than the ppb levels found in a few lunar samples. The consensus is that even these levels are not indigenous to the Moon, but represent terrestrial, meteoritic or cometary contamination (see Section 5.5).

The REE patterns observed in tektites and in bottle-green microtektites are identical to those of terrestrial sedimentary rocks [48]. This fact constitutes strong evidence for a parental terrestrial sedimentary rock, and mineralogical studies indicate that the parent material of tektites was "a well-sorted, silt-size sedimentary material" [56].

The major element chemistry of the bottle-green microtektites remains enigmatic, not resembling that of any common terrestrial or extraterrestrial sample. There is some resemblance between the major element chemistry of bottle-green microtektites and the silicate portion of the mesosiderite meteorite, Estherville, but this interesting similarity does not extend to the rare-earth elements. The Estherville silicate REE pattern is nearly flat at about 3 times chondritic levels, with a small negative Eu anomaly, thus differing from bottle-green microtektite patterns by an order of magnitude.

The microtektite compositions are sufficiently variable to lead Mason [57] to query whether they are related to tektites. Their composition is characterized by high concentrations of refractory elements Mg, Al, Ca and low concentrations of alkali elements in comparison to tektites. They also possess sedimentary-type REE patterns [58]. These characteristics indicate that the bottle-green microtektites may represent a refractory residue following severe heating of the source material. Some of the compositions could

represent material condensed from a vapor phase. During these extreme conditions, few element signatures characteristic of the source rock will survive. However, the REE are notably refractory and could be expected to preserve the evidence of their parental material. Such complex processes may account for their unusual compositions.

One of the characteristic features of the lunar rocks is their great age. The lava floods occurred between 3.8 and 3.2 aeons ago. No younger rocks are known at present, although some very minor activity may have occurred. The uplands were formed between 4.4 and 4.0 aeons ago. All these ages are much greater than those observed for the parent material of tektites. As noted earlier, the tektite-forming events all occurred in the Tertiary or Pleistocene on Earth, as dated by K-Ar or fission track methods. The melting episodes have not seriously disturbed the Rb-Sr or Sm-Nd isotopic systems, enabling ages of the parent material to be assessed. The Ivory Coast tektite data fall on a 2.0×10^9 year isochron defined by the Bosumtwi crater rocks, indicating derivation from that material. The Southeast Asian and Australian tektite Rb-Sr data indicate a Mesozoic age for the parent material. There thus appears to be an order of magnitude difference between the lunar ages and those indicated for the parent material of the Southeast Asian tektites. Recent studies of Sm-Nd isotopic systematics confirm these suggestions. The data are consistent with a terrestrial sedimentary precursor derived from continental crust material for the Australasian tektites [59].

The large young ray craters indicate a frequency of large-impact events on the Moon at about one per hundred million years, about an order of magnitude less frequent than the tektite events. If Tycho were the source of tektites, it should be 0.7 million years old. The current estimate for the age of Tycho is about 100 million years (Section 4.10). Crater counting statistics suggest even older ages.

The $\delta^{18}O$ values for tektites range between +9 and +11.5 per mil. The lunar $\delta^{18}O$ values are low, ranging from +4 for ilmenite to +7 for cristobalite. There is a consensus that the oxygen isotope data are unfavorable to the lunar tektite hypothesis and Taylor and Epstein [60] conclude that "suitable parent materials are rare or non-existent on the lunar surface."

The absence of exposure to cosmic-rays precludes origins from outside the Earth-Moon system, either from elsewhere in the solar system, or outside. The evidence supports the origin of tektites by cometary (or meteorite) impact on terrestrial sedimentary rocks. The chemical, isotopic, and age evidence from the lunar samples enable us to reject the lunar impact hypothesis. A fitting epitaph has been provided by Schnetzler [61]: "The lunar origin of tektites, a controversial and stimulating theory on the scientific scene for almost 75 years, died on July 20, 1969. The cause of death has been diagnosed as a massive overdose of lunar data."

O'Keefe [62] has revived the theory that tektites come from lunar volcanoes, proposing to launch them from a lunar volcano "which should be

powered by hydrogen." This useful fuel, which provided some of the thrust needed for the Apollo lunar missions, is probably scarce on the Moon, except in the lunar soil where it is trapped from the solar wind (e.g., [63]). The composition of lunar rocks is characterized by a depletion in volatile elements and an enrichment in refractory elements. The presence of hydrogen in the amounts needed for volcanic activity in the Moon would be a scientific fact of great significance and would reverse most of the present conclusions about the origin and evolution of the inner solar system (see Chapter 9). Kozyrev [64] reported H_2 emission from the central peak of Aristarchus, which he ascribed to volcanic activity. The central peaks of large impact craters on the Moon are not volcanoes, but result from the impact process, and characterize craters with diameters greater than 10–20 km (e.g., [65]). Kozyrev's observation joins a long list of transient lunar phenomena, observed using earth-based telescopes, but not from the Apollo missions, and which should be treated with caution (cf. Crater Linné controversy, Section 3.14).

Several difficulties attend this volcanic hypothesis. Most of the objections to the lunar-impact theory—based on chemical, age and isotope data—still apply. Our sampling of lunar volcanic rocks does not encourage the view that lavas of tektite composition might be erupted. Such eruptions would need to be among the recent lunar events (<50 million years ago), to account for the tektite ages. If they are powerful enough to accelerate tektite glass beyond the escape velocity (2.4 km/sec) of the lunar gravitational field, then tektite glass or material of tektite composition should occur in the uppermost portions of the lunar regolith. Although many diverse compositions occur among the returned lunar samples, tektite compositions are not among them.

Spherules of meteoritic origin occur in tektites [66]. This and the presence of shocked mineral inclusions indicative of shock pressures far in excess of 100 kbars [57] seems particularly difficult to ascribe to volcanic pressures but highly supportive of an impact origin. The apparent absence of young volcanic vents, or of glassy ejecta of tektite composition on the lunar surface, comprises insuperable problems for the lunar volcanic model. To this may be added the lack of reasonable petrogenetic models capable of generating large volumes of material of tektite composition on the Moon. We may safely conclude that tektites do not come from the Moon.

All the evidence summarized above points unequivocally to an origin for tektites by meteoritic, cometary or asteroidal impact on terrestrial sedimentary rocks.

4.5 Chemistry and Petrology of the Regolith

The average chemical composition of the fine-grain-size (< 1 mm) regolith at the various sites is given in Table 4.3. There are considerable variations

Table 4.3a Major element composition of soils from the Apollo landing sites.†

Apollo:	11	12		14	15		16		17
	10084	12001	12033	14163	15221	15271	64501	67461	70009
SiO_2	41.3	46.0	46.9	47.3	46.0	46.0	45.3	45.0	40.4
TiO_2	7.5	2.8	2.3	1.6	1.1	1.5	0.37	0.29	8.3
Al_2O_3	13.7	12.5	14.2	17.8	18.0	16.4	27.7	29.2	12.1
FeO	15.8	17.2	15.4	10.5	11.3	12.8	4.2	4.2	17.1
MgO	8.0	10.4	9.2	9.6	10.7	10.8	4.9	3.9	10.7
CaO	12.5	10.9	11.1	11.4	12.3	11.7	17.2	17.6	10.8
Na_2O	0.41	0.48	0.67	0.70	0.43	0.49	0.44	0.43	0.39
K_2O	0.14	0.26	0.41	0.55	0.16	0.22	0.10	0.06	0.09
MnO	0.21	0.22	0.20	0.14	0.15	0.16	0.06	0.06	0.22
Cr_2O_3	0.29	0.41	0.39	0.20	0.33	0.35	0.09	0.08	0.41
Σ	99.8	101.0	100.8	99.8	100.5	100.4	100.3	100.8	100.5

†Values given in wt.%.

Sources: Laul, J. C., and Papike, J. J. (1980) *PLC 11:* 1307.
Laul, J. C., et al. (1978) *PLC 9:* 2065.

in chemistry, which reflect the nature of the underlying bedrock. Thus the Apollo 11 soils have high-Ti contents and other characteristics of the Apollo 11 mare basalts. In contrast, the Apollo 16 site, deep within the highlands, is dominated by the high-Al and Ca, and low-Fe and Mg contents of the highland rocks.

The chemical compositions of the soils have been interpreted generally in terms of mixing models. Basic to the problem is the identification of the "end-members" involved in the mixing models. This problem is complex in detail at all sites.

During the formation of the regolith, a wide sampling of the lunar surface occurs. The astronauts' sampling of rocks was necessarily restricted. The aluminous mare basalts, for example, are almost certainly underrepresented in the collections. Thus, it is somewhat surprising that we get such a good match between the regolith and the whole-rock compositions at the mare sites. The more pulverized highlands present less of that particular problem, but put the problem back into a megaregolith stage. Average chemical compositions for the lunar regolith reflect the bedrock differences to be discussed in later chapters and indicate the truth of the comment that there is no large-scale lateral transfer of surface material between highlands and maria.

Increasingly detailed studies have been undertaken on regolith samples, and in particular, much effort has been expended on core studies [67, 68]. Samples restudied include many well-known soils (10084, 12001, 12033, 14163, 15221, 15271, 64501 and 67461).

The petrographic examination clearly indicates the effects of local derivation of much of the material. In terms of pyroxene compositions, 10084

Table 4.3b Trace elements in soils from the Apollo landing sites.†

Apollo:	11	12		14	15		16		17
	10084	12001	12033	14163	15221	15271	64501	67461	70009
Rb	3.2	23	14	14.6		5.7	2.0		
Ba	170	430	600	800	240	300	130	60	120
Pb	1.4		4.0	10		2.8			
Sr	160	140	160	170	120	130	170	170	210
La	15.8	35.6	50	67	20.5	25.8	10.8	4.7	7.9
Ce	43	85	133	170	54	70	28	12	28
Nd	37	57	85	100	36	45	19	7.2	23
Sm	11.4	17.3	22.8	29.1	9.7	12	4.8	2.0	8.1
Eu	1.60	1.85	2.45	2.45	1.30	1.50	1.05	1.00	1.76
Tb	2.9	3.7	4.9	5.9	2.0	2.6	1.0	0.45	1.9
Dy	17	22	30	36	12	—	6.0	2.8	11.4
Ho	4.1	5.0	7.2	8.6	2.9	3.9	1.4	—	2.9
Tm	1.6	1.8	2.6	3.2	1.1	1.4	0.55	0.25	—
Yb	10.0	13.0	17	21	6.9	8.5	3.4	1.6	7.1
Lu	1.39	1.85	2.45	3.00	0.97	1.20	0.49	0.22	1.1
Eu/Eu*	0.37	0.30	0.30	0.22	0.38	0.35	0.60	1.38	0.59
Y	99	—	160	190	86	—	—	—	—
Th	2.1	5.40	8.50	13.3	3.0	4.6	1.85	0.83	0.95
U	0.54	1.7	2.4	3.5	—	1.2	0.4	—	0.23
Zr	320	—	760	850	—	390	—	—	—
Hf	9.0	11.8	16.6	23	6.7	8.6	3.3	1.6	6.6
Nb	118	—	44	46	—	25	—	—	—
V	70	110	100	45	80	80	20	20	100
Sc	60	40	36	22	21	24	8.0	7.8	57
Ni	200	310	210	330	273	220	380	—	—
Co	28	43	34	33	41	41	20	9	32
Cu	10	7.2	8	8	—	9	—	—	—
Zn	23	—	14	34	—	21	—	—	44
Li	10	18	24	27	—	—	—	—	—
Ga	5.1	4.2	3.1	8.3	—	4.4	—	—	6.3
Au, ppb	2.4	2.6	—	5.4	—	4	14	—	3
Ir, ppb	6.9	11	—	14	—	9	12	—	—

†Values given in ppm except where noted.

resembles the Apollo 11 basalts, 12001 is similar to the Apollo 12 olivine and ilmenite basalts. The pyroxenes from soil 14163 correspond to those of Apollo 14 low-K Fra Mauro basalts. Soils 15221 and 15271 have pyroxenes similar to intermediate-K Fra Mauro basalts. Those from 64501 and 67461 are similar to anorthositic rocks. The high-K soil from Apollo 12 (12033) has a pyroxene chemistry similar to Apollo 14 KREEP basalts, confirming its exotic origin. Intrasite mixing of soils is minor. This accords with models of regolith production as a sucession of ejected sheets of debris from impacts, with stirring (gardening) by micrometeorites of the upper layers only. The two Apollo 16 soils do not show any real differences. The finer fraction of the soils

does not contain any preferential enrichment of *exotic* material, except in the Apollo 17 soils, where highland material is enriched in the finer fractions [67, 68]. Average glass compositions are given in Table 4.4.

There is a 20–30% highland component in the Apollo 11 soil, most of which is observed in petrographic studies. The nearest highlands are over 50 km away, and lateral transport is not very efficient. It is suggested that this material is mainly derived by excavation by meteorite craters from beneath the mare basalts. Accordingly, these must be thin [69, 70]. However, we must recall that all the mare basalt landing sites (except Apollo 12) are near the edges of basins, where the basalt flows are thin anyway. Apollo 12, in Oceanus Procellarum, is in an irregular maria, which by definition is thin. Nevertheless, the presence of a thin layer of "light grey fines," 12033, is clearly exotic to the Apollo 12 site, and is usually identified as coming from Copernicus.

Other explanations, such as the occurrence of an earlier stratum of aluminous mare basalts, have been postulated. According to Labotka [67], "There is no evidence, nor any need for the widespread aluminous mare basalts" (e.g., [71]).

The chemistry of the regolith at different sites has been surveyed most recently by Laul and Papike [72]. They find that a major chemical discontinuity appears in the <10 micron fraction. This comprises 10–15% of the bulk soil and is apparently more feldspathic and enriched in highland components, relative to the coarse fractions of the soils. In addition, the KREEP component (Section 5.4.3) is distributed in the soils on a moon-wide basis. Figure 4.13 shows the REE patterns in lunar soils. The bulk composition of highland soils was modelled by Korotev and co-workers [73], using end-member components of KREEP, FAN (ferroan anorthosite), MAF (mafic components) and HON (highlands olivine norite) creating a Disney-like assemblage of characters. Although a 5–10% mare component in the fine fractions of the Apollo 16 soils has been claimed [72], this is probably an artifact of the mixing calculations. There is less than 0.1% mare basalt in the fractions greater than one millimeter in size. The presence of a large fraction of mare basalt at the Descartes site far removed from the maria does not accord with other evidence. The soil composition at the Apollo 16 site is of interest on account of possible differences between the Cayley and the Descartes Formations [74]. However, the soils do not show any distinction in chemical composition [75]. ". . . There are no significant differences between Cayley and Descartes material at the A-16 site . . . " [75, p. 1354]. A general review of the petrology of lunar soils is given by Heiken [76].

4.5.1 Metallic Iron in the Lunar Regolith

The regolith is enriched in metallic Fe relative to its ultimate source material. The origin of this metallic iron is of interest because of its effect on

Table 4.4a Average composition of glass types in Apollo 15 fines.†

		Mare basalt				Highland	Fra Mauro basalt				
	Green glass (%)	Mare 1 (%)	Mare 2 (%)	Mare 3 (%)	Mare 4 (%)	basalt (%)	Low K (%)	Moderate K (%)	High K (%)	"Granite" 1 (%)	"Granite" 2 (%)
SiO_2	45.43	45.70	44.55	43.95	37.64	44.35	46.56	49.58	53.35	73.13	62.54
TiO_2	0.42	1.60	3.79	2.79	12.04	0.43	1.25	1.43	2.08	0.50	1.18
Al_2O_3	7.72	13.29	11.77	8.96	8.46	27.96	18.83	17.60	15.57	12.37	15.73
Cr_2O_3	0.43	0.33	0.26	0.46	0.48	0.08	0.20	0.17	0.12	0.35	0.03
FeO	19.61	15.83	18.83	21.10	19.93	5.05	9.67	9.52	10.25	3.49	6.67
MgO	17.49	11.72	8.84	12.30	10.49	6.86	11.04	8.94	5.77	0.13	2.51
CaO	8.34	10.41	10.46	9.02	8.81	15.64	11.60	10.79	9.57	1.27	6.86
Na_2O	0.12	0.30	0.34	0.27	0.54	0.19	0.37	0.74	1.01	0.64	0.98
K_2O	0.01	0.10	0.13	0.05	0.13	0.01	0.12	0.47	1.11	5.97	3.20
Total	99.57	99.28	98.97	98.90	98.52	100.92	99.66	99.24	98.83	97.85	99.70
No. of analyses	187	67	21	26	6	36	82	90	29	2	1
Percentage of total analyses	34.2	12.2	3.8	4.8	1.1	6.6	15.0	16.5	5.3	0.4	0.2

†From Reid, A. M., et al. (1972) *Meteoritics.* 7: 406.

Table 4.4b Glass compositions in soil from the Apollo 16 site, Descartes.

	Anorthosites		Highland basalt		LKFM	MKFM	High Mg	Mare		Green Glass
	(1)	(2)	(3)	(4)	(5)	(6)	(7)	(8)	(9)	(10)
SiO_2	44.9	48.8	42.0	45.4	46.7	50.8	45.4	46.2	42.0	44.1
TiO_2	0.04	0.08	0.35	0.43	0.75	2.54	0.19	1.76	7.92	0.37
Al_2O_3	35.8	33.4	30.9	27.6	21.5	15.6	15.4	14.3	10.0	7.8
Cr_2O_3	—	—	0.04	0.07	0.11	0.15	0.25	0.29	0.42	0.33
FeO	0.18	0.22	3.46	4.62	6.89	11.1	8.46	14.9	17.0	21.1
MgO	0.12	0.05	6.24	6.13	10.4	7.13	21.1	10.3	10.4	16.7
CaO	19.0	16.3	17.3	15.6	12.9	10.2	9.55	11.0	10.1	8.4
Na_2O	0.55	1.82	0.12	0.42	0.31	0.85	0.17	0.36	0.39	0.13
K_2O	0.03	0.11	0.01	0.05	0.08	0.65	0.01	0.10	0.10	0.03
Total	100.62	100.78	100.42	100.32	99.64	99.02	100.53	99.21	98.33	98.96
No. of Analyses	103	7	30	111	29	13	2	9	2	3
Percentage of total analyses	33	2.2	9.7	36	9.3	4.2	0.6	2.9	0.6	1.0

Source: Ridley, W. I., et al. (1973) *PLC 4*: 309.

Table 4.4c Glass compositions from soils from the Apollo 17 site, Taurus-Littrow Valley.

	Mare						Non-Mare			
	Orange glass		High-Ti		VLT		Anor-thosite	Highland basalt	MKFM	LKMF
	(1)	(2)	(3)	(4)	(5)	(6)	(1)	(2)	(3)	(4)
SiO_2	39.2	39.8	41.7	37.8	46.7	46.6	44.5	45.4	51.0	45.9
TiO_2	8.9	8.9	8.6	11.4	0.72	0.85	0.01	0.39	1.56	1.57
Al_2O_3	5.9	7.9	10.8	8.9	10.4	12.5	35.5	25.4	18.9	19.3
Cr_2O_3	0.67	0.58	0.30	0.39	0.60	0.51	—	0.12	0.13	0.21
FeO	22.4	22.0	17.4	21.8	18.4	18.0	0.20	5.6	8.3	9.2
MnO	0.28	0.29	0.22	0.23	0.24	0.27	—	0.04	0.09	0.10
MgO	14.6	11.3	9.2	9.0	12.7	10.5	0.12	8.0	7.0	10.9
CaO	7.2	8.3	10.9	9.0	9.7	10.5	18.7	14.5	11.2	11.9
Na_2O	0.36	0.41	0.31	0.67	0.18	0.14	0.51	0.24	0.68	0.24
K_2O	0.09	0.09	0.07	0.15	0.03	0.04	0.05	0.06	0.53	0.11
Total	99.6	99.57	99.5	99.34	99.67	99.91	99.59	99.75	99.39	99.43
No. of Analyses	94	11	10	8	42	14	5	64	10	30
Percentage of total Analyses	33	3.8	3.5	2.8	15	4.9	1.7	22	3.5	10

Source: Warner, R. D., et al. (1979) *PLC 10*: 1437.

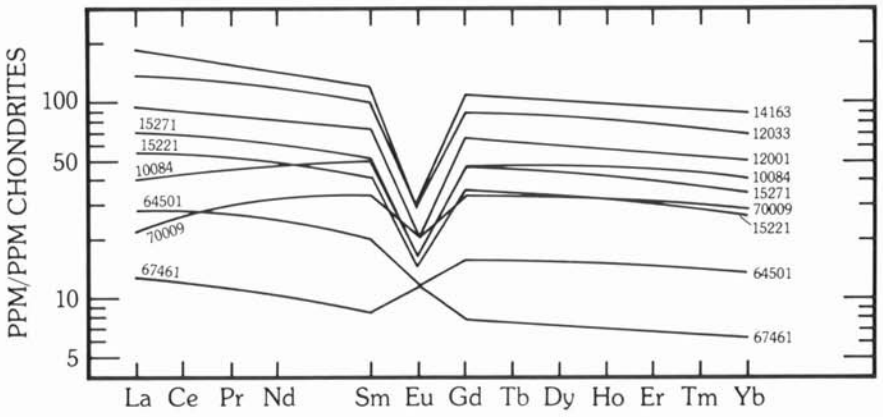

4.13 Chondrite normalized rare-earth element (REE) patterns in soils from the Apollo 11, 12, 14, 15, 16 and 17 landing sites. Note the wide diversity in patterns. Data from Table 4.3b.

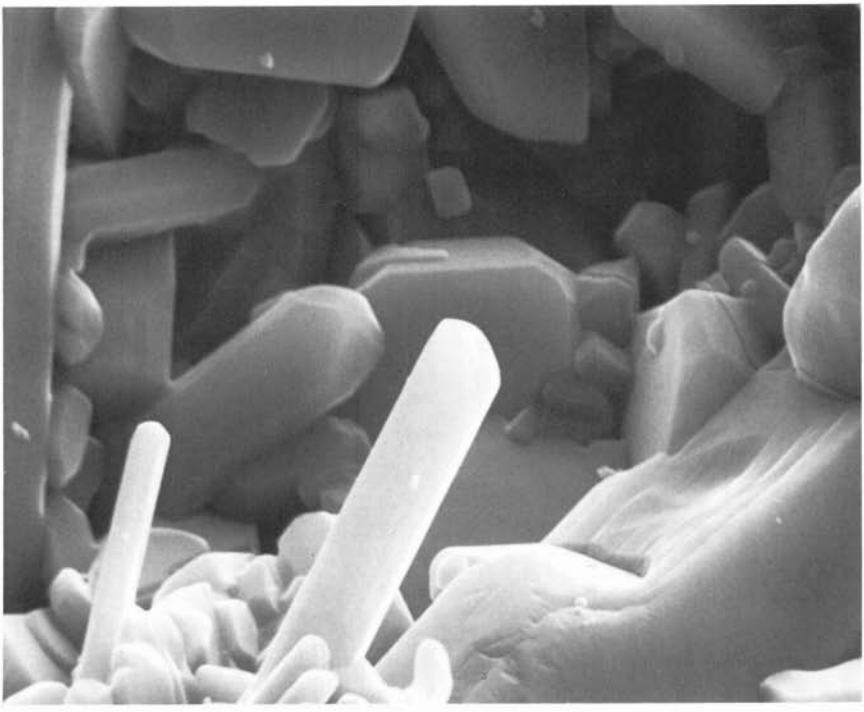

4.14 SEM photograph of a vug lined with crystals in an Apollo 14 lunar breccia. The large pyroxene crystal in the foreground is 8 microns long. Euhedral crystals of apatite, pyroxene and plagioclase form an open network. (NASA S.73-34448. Magnification 3000X. Courtesy D. S. McKay.)

lunar magnetic properties (see Section 7.8). There is general agreement that this "excess" metal is produced by lunar surface processes [77–79].

There are three sources of metallic iron particles in the regolith [80]. These are: (a) Metal particles produced from reduction of ferrous iron induced by exposure. These are mainly associated with agglutinates, and range in size between 40–330 Å. (These particles are derived by reduction of Fe^{2+} in silicate and oxide phases). (b) Metal particles from micrometeorites involved in the formation of agglutinates. These are larger, being mainly >330 Å in diameter, and comprise generally less than about 30% of the metallic fraction. (c) Metallic particles derived from the source rocks for the soils. These are also in general > 330 Å in diameter.

4.5.2 Volatile Element Transport on the Lunar Surface

There is a considerable body of evidence which indicates volatile element mobility, such as the occurrence of vapor phase crystals in cavities and vugs in breccias (Figs. 4.14, 4.15). Such movement of chemical elements on the Moon

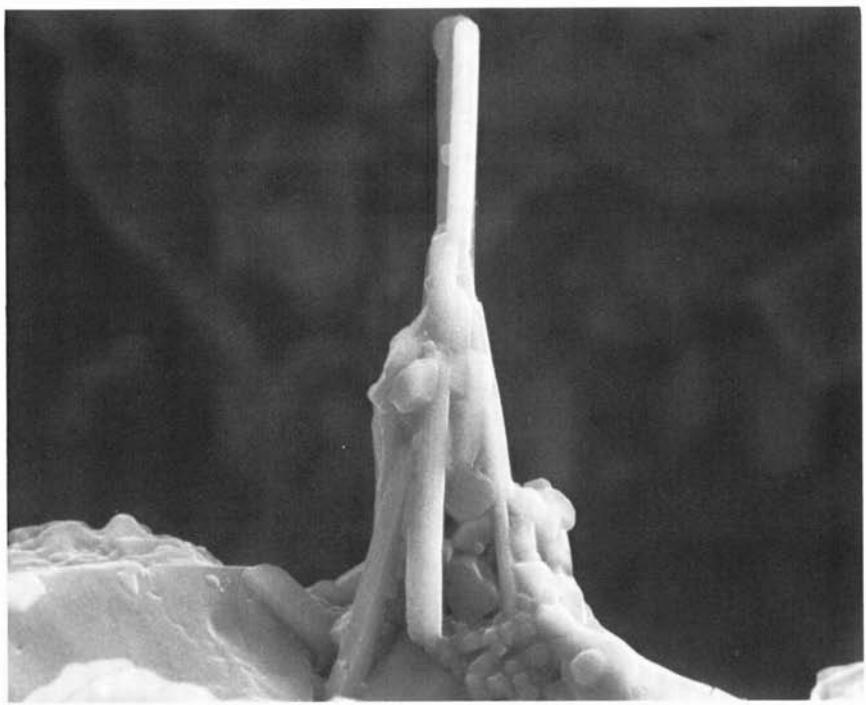

4.15 SEM photo of an isolated pyroxene crystal in a vug in an Apollo 14 breccia. (NASA S.73-34441. Magnification 6000X. Courtesy D. S. McKay.)

may occur by the following processes:

(1) fire-fountains;
(2) solar-wind sputtering;
(3) redistribution of volatiles during meteorite impact.

Volatile elements such as Cd, Zn, In and Ga increase by factors of 10–20 from coarse (500 micron) to fine grain (< 5 micron) sizes. This surface correlated effect indicates selective movement of volatiles during regolith evolution. Trace siderophile elements peak in the 80–300 micron grain size (typical of agglutinate fractions) so that agglutinate formation must involve incorporation of the siderophiles from the meteorite bombardment [81]. Indeed, very moderate temperatures can lead to volatilization and movement of elements on the lunar surface [82]. Hg is probably volatile during lunar daytime conditions when the temperature reaches 130° C, with recondensation at night when the temperature drops to −170° C. Therefore, Hg might be expected to be ubiquitous on regolith grains. Temperatures as low as 250° C cause mobilization of other elements under laboratory conditions [82]. The following elements are enriched on the surfaces of regolith grains: Au, Br, Cd, Ga, Ge, Hg, In, Pb, Sb, Te and Zn. Stepwise heating experiments reveal the following sequence of volatility: Hg≫Cd>Zn>Se>In>Br≫Ag.

These elements are enriched both on the surfaces of mineral grains and especially on agglutinates. These results must engender caution about the interpretation of volatiles on the green and orange glass spheres (Section

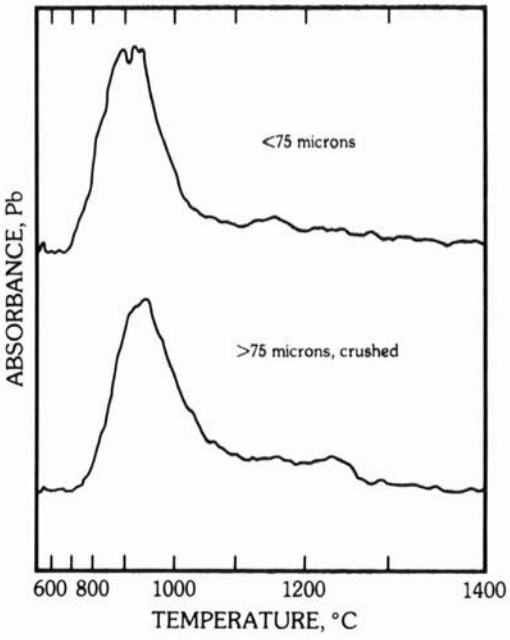

4.16a Thermal release profiles of Pb in rock sample 66095 showing that most of the Pb in both < 75 μm and >75 μm fractions is released below 1000°C before the sample melts and therefore is surface Pb.

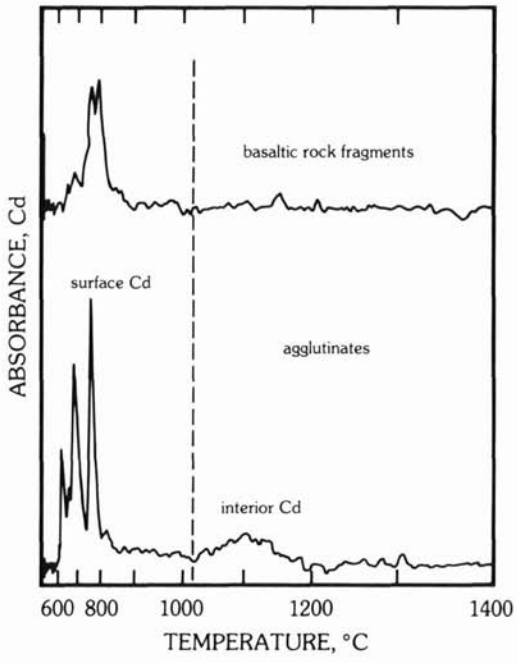

4.16b Cd release profiles of basaltic rock fragments and agglutinates from 150–420 μm size fraction of submature mare fines 75081. Note very little or no interior Cd is present in basaltic rock fragments, whereas some interior Cd is present in agglutinates.

6.2.3) as being uniquely indicative of a volcanic origin [83] since micrometeorite impact will readily volatilize these elements. In this context, volatiles were deposited on the orange glass spheres from Apollo 17, after the spheres had been broken. This is interpreted to have occurred during the formation of

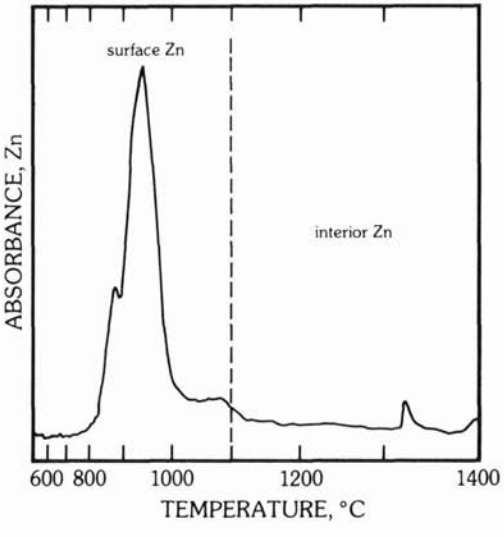

4.16c Thermal release profile of Zn in a pristine anorthosite 65325 showing that most of the Zn is on surfaces.

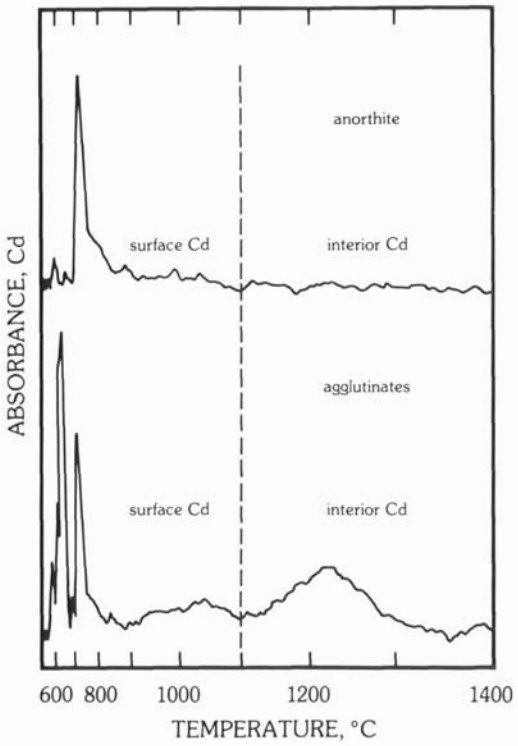

4.16d Thermal release profiles of Cd in anorthite grains and agglutinates from 150–420 μm size fraction of the most mature fines sample 65701. Cd in the anorthite fraction is almost all on grain surfaces. On the other hand, a fair amount of interior Cd as well as surface Cd is present in the agglutinates [85]. (Courtesy R. M. Housley.)

Shorty crater. This event must also have redistributed the volatile elements [84, 85]. Large meteorite impacts will provide enough energy to promote widespread volatile transport across the face of the Moon, although this is restricted to the very surface. However, since most of our returned samples come from this environment, caution should be exercised about the fundamental petrological significance of volatile coatings on glass spheres. The sample investigated by Wegmüller [82] (75080, from the rim of the Camelot crater) contained very few orange or black spherules. Some Cd was volatile at 250° C, Zn and Se at 450° C and Br and In at 650° C. The nature of the volatile compounds is not yet established (Fig. 4.16).

The effects on isotopic systematics, particularly for lead, but also for Rb distribution, need also to be borne in mind. Loss of volatile Rb relative to involatile Sr causes old apparent ages, as are observed on some agglutinate samples [37]. Na and K as well as Rb are mobile [86]. K/Rb ratios are altered at temperatures above 1000–1200° C. Some spherules have surface enrichment of Na and K [87]. Sulfur is even more volatile with 12–30% being lost at temperatures as low as 750° C [86].

Such movement of volatile elements on the lunar surface raises questions about the existence of traps in permanently shadowed regions. Water might

be trapped as ice in craters in polar regions [88]. The source of the water could be from solar wind hydrogen as a source for reduction of FeO, carbonaceous chondrites or cometary impacts, since no unequivocal identification of indigenous water has been made. Other suggestions include the possibility of trapped frozen gases, for example, radon-222 derived from radioactive decay of uranium [89].

4.5.3 The Meteoritic Component

Addition of meteoritic material to the Moon is derived from three sources: the ancient heavy bombardment, young crater forming events, and micrometeorites in addition to possible cometary material. In this section, the nature and composition of the meteorite contribution in the lunar regolith is explored, while the question of the nature of the basin-forming projectiles is discussed in Section 5.6. The investigation of this component was aided by two geochemical factors [90]. The first was the strong depletion of siderophile elements (e.g., Ni, Ir, Au, Re) in the lunar rocks. Such depletions are to be expected on the surfaces of differentiated planets; however, the extreme depletion of the Moon in volatile (and chalcophile) elements (Ag, Bi, Br, Cd, Ge, Pb, Sb, Se, Te, Tl, Zn) enabled the use of these elements, which are relatively abundant in C1 meteorites, as indexes of the meteoritic component. Typical data are shown in Fig. 4.17 for mature soils, with high surface exposure ages. Such soils from all sites give the same result. The meteorite component appears to be similar to C1 chondrites, and the concentration level is 1.5–2% by weight. There is some variability among the volatile constituents, probably due to their mobility in the soils, hence producing a sampling problem. It is of interest that this chemical signature virtually eliminates all the other meteorite classes (irons, stony irons, ordinary chondrites, achondrites) from consideration [90, 91]. Mean influx rates have been calculated as 2.4×10^{-9} g/cm^2/yr. [90] and 2.9×10^{-9} g/cm^2/yr. [91]. Discrepancies between these estimates and those calculated from the microcrater population (0.2×10^{-9} g/cm^2/yr.) [92], which are an order of magnitude less, are discussed in the next section.

4.6 Microcraters and Micrometeorites

The lunar surface is a particularly fine recorder of micrometeorite impacts. This arises from the ubiquitous presence in the regolith of glasses, whose smooth surfaces provide an ideal recording surface for micrometeorite impacts. Typically, these will contain about 5000 microcraters (with diameters of a few microns) per square centimeter. The number of craters decreases with increasing diameter. These microcraters or "zap pits" which occur on rock and

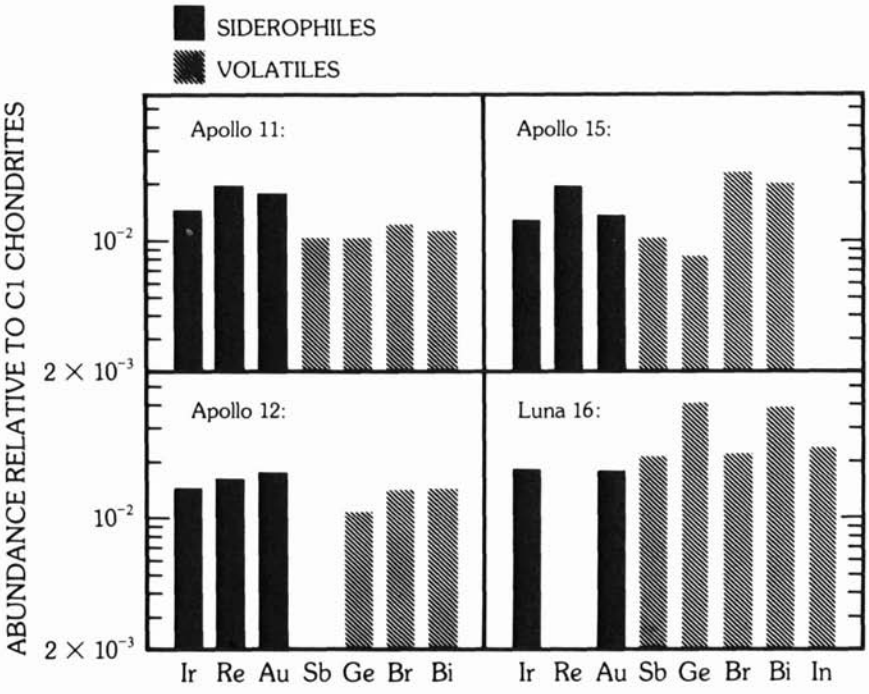

4.17 All mare soils are enriched in "meteoritic" elements, relative to crystalline rocks. Net meteoritic component is obtained by subtracting an indigenous lunar contribution estimated from crystalline rocks. Abundance pattern is flat, with siderophiles and volatiles almost equally abundant. The meteoritic component has a primitive C1 composition [90]. (Courtesy E. Anders.)

mineral surfaces, as well as on the glass spheres, are spectacular (Fig. 3.1). They range in size from less than one micron to more than one centimeter.

Information on the nature of the projectiles provides data on micrometeorite flux and on the nature and composition of "interplanetary" or "cosmic" dust. The microcraters larger than about 3 microns typically consist of a glass-lined pit, and a "spall" zone concentric to the pit (Fig. 4.18). Spallation in this zone will sometimes leave the glass-lined pit standing on a pedestal of "halo" material. The hypervelocity nature of the impacts indicates that "primary" cosmic dust particles [93] are involved rather than "secondary" particles resulting from lunar impacts [94]. Most of these microcraters are compatible only with impact velocities of the dust grains greater than 3.5 km/sec, the actual average velocity being about 20 km/sec.

What conclusions can be drawn about the nature of the particles from the crater morphology? The densities lie within the range 1–7g/cm^3, peaking in

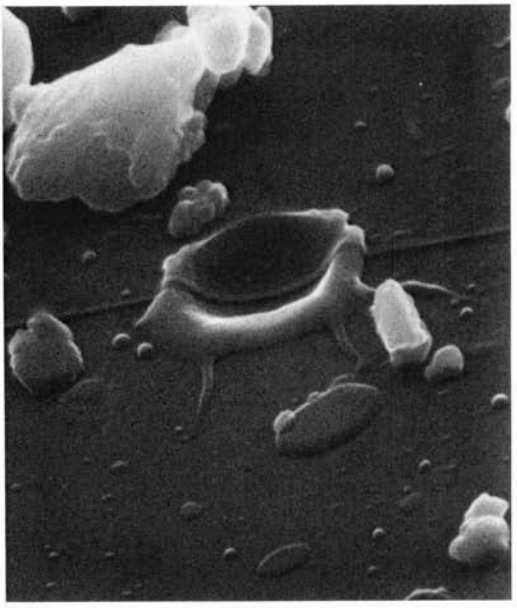

4.18 One-micron sized zap pit on a lunar glass spherule. (NASA S.73-18445. Courtesy D. S. McKay.)

the range 1–2 g/cm^3. Thus, there is a lack of iron particles, and the composition is similar to that of Type I carbonaceous chondrites. These data are consistent with the properties of "Brownlee" particles collected by high-flying aircraft [95].

Therefore, the "model" micrometeorite is non-porous, equant in shape, with a density of 1–2 g/cm^3 with C1 element abundances, including finely dispersed carbon. This observation has implications for theories of cosmic dust origin and early planetary condensation and accretion. The abundance of "frothy" rims on impact pits is consistent with impacts of hydrated phyllosilicates, common constituents of carbonaceous chondrites. The higher density objects (5 g/cm^3) are probably magnetite grains. The most frequent mass range for the particles is from 10^{-7} to 10^{-4} g.

Craters from 1 mm to 100 microns in diameter correspond to a mass ranging from 10^{-3} to 10^{-6} g. Those craters with diameters from 100 to 0.1 microns are caused by particles in the mass range 10^{-6} to 10^{-15} g. Those in the size range 10^{-6} to 10^{-2} g contribute the most energy and are responsible for most of the damage to the rock surfaces. The production rate is about five craters per square centimeter per million years (with diameters > 0.05 cm). Thus, surfaces are effectively saturated at about one million years, and this limits the microcrater technique for exposure-age estimation. The impacts cause erosion, ionization, vaporization, and lateral small-scale transport but little vertical mixing. The erosion rate is of the order of 1 mm per million years [96].

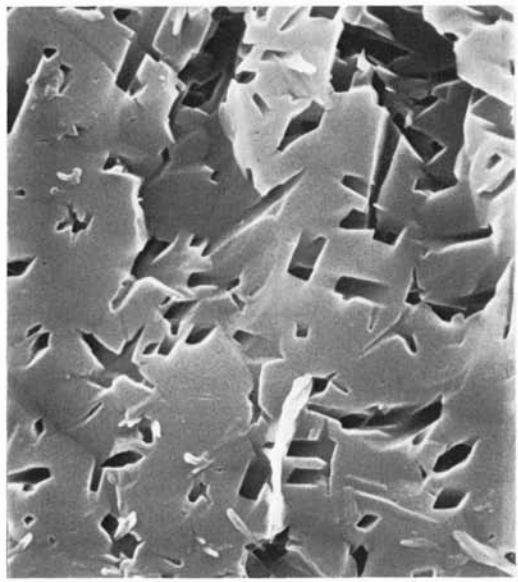

4.19 Etched pits, about one micron across, caused by solar flare iron group nuclei, in an Apollo 14 feldspar. The rectangular outlines of the etched pits are presumably due to crystallographic factors. (NASA S.72-55177. Courtesy D. S. McKay.)

The microcratering effects extend down from those caused by micrometeorites to sputtering by solar wind ions (Fig. 4.19). Table 4.5 indicates the density of microcraters spanning this range. The erosion rate due to the sputtering is about 10^{-8} cm (1Å) per year in the near surface (< 0.1 cm) regions, or about 0.1 mm per million years. This is about one-tenth of the mass erosion rate caused by micrometeorites.

Table 4.5 Microdensities due to micrometeorite impact and solar wind sputtering.

	Crater Diameter	Crater Density (per cm^2)
Micrometeorites	$\geqq 0.3$ mm	20
	$\geqq 0.1$ mm	70
Solar wind sputtering	$\geqq 1$ micron	1000–3000
	$\geqq 0.25$ micron	10,000

The impact velocities of meteoritic dust particles vary from 2.4 km/sec to 74 km/sec. Meteorites larger than 50 g should produce a detectable signal on the lunar seismometers [97]; however, the seismometers have not detected increased flux rates on the Moon at times when meteorite showers have been observed striking the Earth. Since most showers of micrometeorites consist of particles ranging from 1 to 10^{-6}g (F. Hörz, pers. comm, 1981), the failure to detect increased flux rates on the Moon is most likely due to the fact that only

the larger events are recorded (about one signal per day due to meteorite impact [97]).

4.7 Irradiation History of the Lunar Surface

The lunar surface is not excelled as a detector and recorder of solar and cosmic radiation over geological time scales. It is much superior to meteorites, since it has been in its present orbit for a long time, whereas the orbits and dynamical evolution of meteorites are uncertain, extending probably inside the orbit of Venus and out to the asteroid belt. The orbits of two chondritic meteorites, Pribram and Lost City, photographically recorded during entry, indicate an elliptical orbit extending to the asteroid belt. These data help to dispose of the myth that meteorites come from beyond the solar system.

Three types of radiation interact with the lunar surface. In order of increasing energy, these are: (a) solar wind, (b) solar flares, and (c) galactic cosmic rays. The composition of this radiation is similar, being mainly composed of protons, with about 10% helium nuclei and about 1% of nuclei heavier than helium. There are, however, dramatic differences in energy, by many orders of magnitude, and, accordingly, in the effects on the lunar surface. In contrast, the number of particles is inversely proportional to their energy (Table 4.6).

4.7.1 Solar Wind

The solar wind has an average velocity of 400 km/sec with an energy of about 1 keV/nucleon (Table 4.6). The average density at one Å is about 10 ions/cm^3. This plasma, which continually flows outward from the sun, probably represents the composition of the solar corona. Ions are directly implanted into the surfaces of lunar materials, to depths of about 500 Å. The solar wind also causes some surface damage, resulting in some fine-scale rounding and production of an amorphous coating about 400 Å thick on the surfaces of grains [98]. The abundances of the rare gases in the solar wind, relative to hydrogen, approximate the average solar photosphere and coronal abundances [99, 100]. The composition of the solar wind, and its significance for the history of the sun, is discussed in Section 4.11.

4.7.2 Solar Flares

These have higher energies than those of the solar wind, typically in the range of 10 keV to 100 MeV/nucleon (Table 4.6). They occur as short bursts of radiation and there is some correlation with the eleven-year sunspot cycles.

Table 4.6 Nuclear particle effects in lunar samples and meteorites.[†]

Radiation Source	Proton Flux ($P/cm^2/sec$)	Energy	Typical Penetration Distance	Major Observable Effects
Solar wind	3×10^8	1 keV/nuc	300 Å	Direct implantation (e.g., surface correlated rare gases) Re-implantation of lunar atmospheric species (e.g., ^{40}Ar excess in lunar soils) Radiation damage (e.g., amorphous layers on lunar dust grains)
Solar flares	10^2	<1 MeV/nuc to $\geq$100 MeV/nuc many more low energy than high energy particles	millimeter to centimeter	Radionuclide production (e.g., ^{26}Al, ^{53}Mn) Track production (principally tracks produced by slowing down VH nuclei) Electronic defects (e.g., thermoluminescence)
Galactic cosmic rays	1	$\geq$100 MeV/nuc typically~3 GeV/nuc	centimeter to meter	Radionuclide production Stable isotope production (e.g., ^{21}Ne, ^{15}N) Nuclear effects due to buildup of nuclear cascades with depth (e.g., N-capture in Gd) Tracks (spallation recoils in addition to slowing down heavy nuclei)

[†]Adapted from Walker, R. M. (1980) *Ancient Sun*, p. 11.

Solar flares produce three identifiable effects: (1) directly implanted ions, (2) cosmogenic nuclides and (3) nuclear tracks.

The Apollo missions were well timed. Large solar flares occurred in November, 1968, and April, 1969, before the Apollo 11 mission in July, 1969. Large flares were absent before the Apollo 15 mission. A small solar flare, which enhanced the particle flux by a factor of 10^3, occurred during the Apollo 16 mission. In August, 1972, before the December, 1972, Apollo 17 mission, the most intense solar flares observed during the past fifteen years occurred. Tracks produced by solar flares dominate the upper one millimeter of lunar materials that have been exposed directly to sunlight. These track densities are high (10^7–10^9/cm^2).

4.7.3 Galactic Cosmic Rays

These very high energy particles (10^2–10^4 MeV/nucleon) are derived from outside the solar system (Table 4.6). These particles are not implanted in the lunar surface materials since they undergo nuclear interactions due to their high energies. Cosmic ray tracks are produced by the VH ions ($Z = 18$–28) and VVH ions ($Z > 28$), while the lighter nuclei (protons and He nuclei) produce both stable and radioactive isotopes.

There are two main classes of phenomena which result from the interaction of cosmic rays with the lunar surface: (a) solid-state damage as a result of penetration of ionizing particles, producing etchable tracks, and (b) production, through nuclear interactions, of new isotopic species. These effects have been pursued by different investigators using etching and microscopic techniques to study the tracks produced, and mass spectrometric and radiochemical procedures to investigate the cosmogenic isotopes.

4.8 Physical Effects of Radiation

The solar wind causes only minor damage, as noted earlier, producing amorphous surface layers a few hundred angstrom units thick on grain surfaces. Helium nuclei are thought to be mainly responsible [101–103]. The time needed to produce this amorphous layer is about 100 years. Solar flares, in contrast, produce high track densities, sometimes exceeding 10^{11} tracks/cm^2. These are observed even in the deepest core samples, indicating that this material was once at the surface. Such tracks are also observed in gas-rich meteorites [104], although both track densities and the number of grains irradiated by solar flares are less, consistent with much lower rates of surface overturn (gardening) on asteroidal surfaces compared with the lunar regolith.

The tracks produced by galactic cosmic rays are mostly caused by the heavier ions, dominated by the VH ions ($Z = 18$–28) of which iron is the most

abundant species [105]. The track densities fall off steeply with depth, but tracks due to cosmic rays may reach depths of 20 cm or so, in contrast to the predominance of tracks from low energy solar flare ions in the upper one millimeter. Track lengths differ in differing minerals, in the order feldspar > pyroxene > olivine. The tracks are produced only toward the end of the penetration.

Workers have used either the total etchable track length or the track etch rate to identify the nature of the particles. The track length is, in principle, simply related to atomic number, but it has proven difficult to apply in practice [105,106]. Measurement of the track etch rate has been more useful and indicates that there appears to be no sharp threshold ionization value. Tracks from light ions ($Z<18$) etch more slowly than those from heavier ions, and they are more readily erased by thermal annealing [105, 106].

The interpretation of nuclear track data is model dependent "due to erosion of grains by impact and sputtering, or to fading of the tracks over long intervals of time" [107]. This erosion is of the order of one angstrom per year, by sputtering, and one millimeter per million years by micrometeorite impact. Thus, only those surfaces that escape the sputtering and erosion processes yield meaningful data about exposure ages. The intensity of the irradiation is shown by these few uneroded surfaces. A millimeter-sized crystal at the bottom of a vug from an Apollo 15 rock [108], estimated to have been uncovered and exposed about 2×10^4 years ago, has a track density of 5×10^{10} tracks/cm^2 on its surface, and some soil grains that have escaped sputtering have surface track densities of 10^{11}/cm^2. Unshielded rock and grain surfaces have track densities typically about 10^8 tracks/cm^2. Because of experimental difficulties, the error in track counts from different investigators is on the order of $\pm 20\%$ [105].

The cosmic-ray-produced tracks need to be distinguished from fission tracks due to ^{238}U and to ^{244}Pu. High uranium concentrations can contribute more than 10^8 fission tracks/cm^2 at grain boundaries or in inclusions. Their non-uniform distribution, differing etch pit characteristics, and the low fission track density in common minerals (where uranium is low in abundance) enable them to be distinguished from the cosmic ray tracks. Tracks due to the spontaneous fission of ^{238}U are commonly observed, but those from ^{244}Pu (half-life of 82×10^6 yr.) are difficult to find in lunar rocks. Most of the mare basalts are too young to contain measurable amounts of decay products. A slightly more favorable environment exists in uranium-rich mineral phases in the older lunar rocks. Tracks due to ^{244}Pu fission occur in a whitlockite crystal from the Fra Mauro breccias (14321) [109]. This sample was heavily shielded from cosmic rays until about 25 million years ago.

The possible existence of superheavy elements has been much debated. The principal evidence adduced was the presence of long fission tracks. These >20 micron tracks, which were identified as being due to extinct superheavy elements, are probably "fresh" tracks due to cosmic ray nuclei. There is no

definitive evidence for the existence of the superheavy elements around Z = 114 [107].

Despite all the complications, the track record produces very useful results. A principal conclusion in this section is that the galactic cosmic ray flux has been effectively constant over the past 50 million years. It becomes difficult to extrapolate this conclusion much beyond this age from the track data because of the increasingly important effects of erosion [110].

4.9 Chemical and Isotopic Effects

The reaction of the lunar surface materials with the solar and galactic radiation causes many changes in chemical abundances. Hydrogen in lunar soils is nearly devoid of deuterium, which is destroyed in nuclear reactions in the sun. Accordingly, the hydrogen is of solar, not lunar (or terrestrial) origin [111].

4.9.1 Carbon, Nitrogen and Sulfur

The overall average carbon content of lunar rocks is 30 ppm, but the soils average 115 ppm [112, 113]. Of this, about 5–10 ppm may be accounted for from meteoritic or cometary sources and the remainder is derived from direct implantation by the solar wind. The finest grain sizes contain the highest concentrations, and this "surface correlated" effect is usually considered to be evidence of an extra-lunar component. However, this concept should not be applied too widely, since the surfaces of many grains are coated with glass splashes. Unlike the rare gases, carbon is reactive and this has made study of the isotope ratios difficult on account of fractionation effects.

Nitrogen, like carbon, is mainly of extra-lunar origin. The average concentration in igneous rocks is less than one ppm [114, 115]. Higher values [116, 117] are due to atmospheric contamination. The soils range from 50 to 100 ppm and average 82 ppm. The low content of nitrogen in lunar rocks is consistent with the overall depletion of the Moon in volatile elements. Nitrogen appears to be retained more quantitatively than the noble gases, H or C [118] and is thus a better measure of the integrated solar wind flux. A significant change in the isotopic composition has occurred, with $^{15}N/^{14}N$ decreasing at a rate of 15% per billion years. The only viable hypothesis appears to be that of a secular change in the solar wind [119, 120].

Sulfur is relatively abundant in lunar rocks, averaging about 1000 ppm, where it is present as troilite (FeS). An extra-lunar component has been identified in the soils, which have about the same abundance levels [116, 121]. The isotopic fractionation of sulfur in lunar soils indicates relative enrichment in the heavy isotopes [122] similar to that of the heavy isotopes of oxygen,

Table 4.7 Comparisons of rare gas contents (cm^3 STP/g) and elemental ratios of regolith fines, the solar wind and the terrestrial atmosphere.

Site	^4He 10^{-2}	^{20}Ne 10^{-4}	^{36}Ar 10^{-4}	^{84}Kr 10^{-8}	^{132}Xe 10^{-8}	($^4He/^{20}Ne$)	($^{20}Ne/^{36}Ar$)	($^{36}Ar/^{84}Kr$) $\times 10^3$	($^{84}Kr/^{132}Xe$)
Apollo 11	11–25	20–31	3.3–4.1	16–38	2.1–10	55–104	5.2–9.2	1.0–2.2	2.1–8.6
Apollo 12	4–38	7–61	1.2–3.1	4–20	1.1–2.6	55–72	4.9–6.6	1.2–3.1	3.5–8.5
Luna 16	18	34	5.4	22	8.5	53	6.3	2.5	2.6
Apollo 14	5–9	9–16	2.4–4.4	9–24	1.4–4.6	52–64	3.0–4.2	1.6–2.8	3.6–12
Apollo 15	4–10	7–22	0.9–4.1	4.4–24	0.6–3.3	38–58	4.4–7.7	1.5–2.9	4.8–8.1
Apollo 16	0.6–5.1	2.4–13	1.3–6.0	4.5–34	1–6.5	26–50	1.6–3.2	1.5–3.2	2.3–7.2
Luna 20	3.81	10.1	2.88	10.9	2.25	32–39	2.4–3.5	2.6–3.0	4.8–6.6
Apollo 17 ("mare")	12–29	14–45	1.6–6.2	3.7–16	1.3–2.4	53–117	4.9–9.3	2.2–4.3	2.8–6.5
Apollo 17 ("highland")	5.9–16	12–28	2.5–4.9	10–18	1.8–2.9	40–64	4.4–5.8	2.4–2.8	5.4–7.2
Solar wind composition experiment	—	—	—	—	—	570 ± 70	28 ± 9	—	—
Terrestrial atmosphere	—	—	—	—	—	0.3	0.5	—	—

Sources: Walton, J. R., et al. (1973) *PLC 4:* 2086.
Heymann, D. (1977) *PCE* 10: 47.
Bogard, D. D., and Nyquist, L. E. (1972) *PLC 3*: 1804.
Geiss, J., et al. (1972) NASA SP 315, 14-1.

silicon and potassium. Sputtering by micrometeorite bombardment is usually considered as the dominating process.

4.9.2 The Rare Gases

The concentration of rare gases in the lunar fines is typically in the range 0.1–1.0 cm^3 STP/g, corresponding to about 10^{19}–10^{20} atoms/cm^3. These are very large amounts and were one of the surprises encountered during the Apollo 11 Preliminary Examination Team study. The detailed composition of the gases is given in Tables 4.7 and 4.8 [123].

Table 4.8 Isotopic composition of trapped rare gases in the lunar regolith compared with solar wind and terrestrial atmospheric values.

	$^4He/^3He$	$^4He/^{20}Ne$	$^{20}Ne/^{22}Ne$	$^{22}Ne/^{21}Ne$	$^{20}Ne/^{36}Ar$
Bulk lunar fines	2300 – 2800	96 ± 18	12.4 – 12.8	31 ± 1.2	
Solar wind	2350 ± 120	570 ± 70	13.7 ± 0.03	30 ± 4	28 ± 9
Terrestrial atmosphere	7×10^5	0.3	9.8 ± 0.08	34.5 ± 1.0	0.5

Sources: Bogard, D. D., and Nyquist, L. E. (1972) *PLC 3*: 1804.
Geiss, J., et al. (1972) NASA SP 315, 14-1.
Heymann, D. (1977) *PCE* 10: 49.
Eberhardt, P., et al. (1972) *PLC 3:* 1821.

The location of such large volumes of gas is intriguing. The gas occurs in bubbles, typically 50–100 Å in diameter in soil grains, under high (~5000 atm) pressures [108]. The penetration of the solar wind as shown by surface etching is on the order of 1000 Å, while the solar flare ions penetrate to millimeter depths. The rare gas contents increase with decreasing grain size.

On the Moon, there is no evidence of rare gases that might be residual from a primitive atmosphere. This is consistent with the general depletion of volatile elements, and, based on the low abundances of elements such as Pb and Tl, it may safely be concluded that the primordial rare gas content of the Moon was effectively zero and that any primitive isotopic signature is swamped by the later effects.

Thus, the large quantities of rare gases found, particularly in the lunar soils, must be of secondary origin. The rare-gas inventory records a complex variety of origins. Although these relate to differing processes (e.g., solar wind trapping, cosmic ray interaction, fission products, and radioactive decay), it is convenient and customary to treat the rare-gas studies as a group, which reflects the historical development of the studies.

There are several distinct sources for the rare gases observed in lunar surface samples. These include the following:

(a) trapped solar wind ions;
(b) implanted solar flare ions;
(c) isotopes produced by solar proton spallation and by high energy cosmic ray interactions (e.g., ^{3}He, ^{21}Ne, ^{38}Ar);
(d) isotopes from radioactive decay (e.g., ^{40}Ar from ^{40}K);
(e) fission-produced isotopes (e.g., ^{131}Xe from ^{244}Pu fission);
(f) neutron capture produced isotopes (e.g., ^{131}Xe from ^{130}Ba).

Trapped He and Ne are richer in soils from the maria compared to those of the highlands. This effect appears to be due to the superior trapping efficiency of iron- and titanium-bearing minerals (e.g., ilmenite compared with plagioclase [123]). He and Ne are generally depleted relative to the heavier gases (Ar, Kr and Xe) compared to solar abundances.

4.9.3 The Argon-40 Anomaly

There are about two orders of magnitude excess of ^{40}Ar in the lunar soils compared with the amount expected from solar wind trapping and ^{40}K decay. Early suggestions were that ^{40}Ar atoms, resulting from the ^{40}K decay, escape from the lunar surface and are ionized by solar radiation [124, 125]. After ionization, the particles are then subject to rapid acceleration by the magnetic fields associated with the solar wind and strike the lunar surface with energies of 100–1000 keV within a few seconds. At low energies, they are neutralized but not trapped, and hence recycled. Ions with impact energies greater than 1 keV are trapped in the fines, thus building up an excess of ^{40}Ar.

The apparent absence of excess ^{40}Ar in near-surface regions of grains, and the apparently low amounts of ^{40}Ar released at low temperatures, led to alternative suggestions that potassium, volatilized during impact, coated the grain surface and produced the excess ^{40}Ar [126, 127].

It has also been argued that most of the excess argon was implanted 3–4 aeons ago and that calculations based on the present-day flux, solar wind, and magnetic fields are not relevant [128]. However, it is probable that the initial suggestions with regard to the mechanism for trapping argon are correct [124, 125].

The meteoritic gas-rich breccias greatly resemble lunar soil breccias [104, 130]. The exposure of meteorites to cosmic ray bombardment produces cosmogenic (= spallogenic) noble gases, especially ^{3}He, ^{21}Ne and ^{38}Ar, which may be used to calculate exposure ages, assuming a production rate of 2.39×10^{-8} ^{3}He STP/g/million years (see Section 4.10). The significant differences in rare gas contents among the atmospheres of the Earth, Venus and Mars are discussed in Section 4.13 [130].

4.9.4 Cosmogenic Radionuclides

A wide variety of nuclides are produced by the solar flare and galactic cosmic ray interaction with the lunar surface [106, 107, 131], ranging from ^{52}Mn with a half-life of 5.6 days to the geologically more useful ^{53}Mn with a half-life of 3.7 million years (Table 4.9). At the surface, the solar flare protons account for most production, but below about one centimeter, secondary particles from the galactic cosmic rays dominate. There is accordingly a strong depth dependence. There were no observable differences at the Apollo 16 site between samples collected from the Cayley and the Descartes Formations. This result is consistent with the absence of chemical variation observed at the site. Work on some of the larger rocks shows that the contribution from galactic cosmic rays can be separated at depth from the solar cosmic radiation [132, 133].

Production of ^{236}U (half-life of 2.34×10^7 yr.) and ^{237}Np (half-life of 2.14×10^6 yr.) by solar proton reactions with ^{238}U have been reported [134]. The difference in the half-lives of ^{236}U and ^{237}Np provides a monitor of solar cosmic ray activity by comparison of the ratios. Although no direct evidence of plutonium was found, the fission track evidence in uranium-rich minerals such as whitlockite points to its presence [109].

4.9.5 Thermal Neutron Flux

The low-energy thermal neutrons produced by the cosmic ray bombardment result in anomalous isotopic abundances for those nuclides with large thermal neutron capture cross sections. Those most commonly measured are ^{158}Gd (from ^{157}Gd), ^{156}Gd (from ^{155}Gd), and ^{150}Sm (from ^{149}Sm). The neutron flux with depth was measured by a neutron probe, using the ^{10}B capture rate and ^{235}U induced fission rate, on the Apollo 17 mission [135, 136]. The neutron fluxes measured on the returned samples are low compared with those expected for a well-mixed regolith; the data are consistent with non-uniform mixing, in that the material toward the base has undergone more irradiation. Since the depth of penetration of neutrons is of the order of a meter or so, this is a reasonable conclusion, consistent with regolith formation models which add fresh layers of material to the top.

4.10 Exposure Ages and Erosion Rates

The record from nuclear tracks and the rare gas data can be employed to determine exposure ages of rocks and soils, providing valuable evidence for

Table 4.9a Radionuclides commonly detected in lunar samples and meteorites.

Radionuclide†	Half-life (yr.)	Targets
^{3}H	12.33	O, Mg, Si
^{10}Be	1.6×10^{6}	O, Mg, Si
^{14}C	5730	O, Mg, Si
^{22}Na	2.60	Mg, Al, Si
^{26}Al	7.3×10^{5}	Al, Si
^{36}Cl	3.0×10^{5}	Ca, Fe
^{37}Ar	0.095	Ca, Fe
^{39}Ar	269	K, Ca, Fe
^{46}Sc	0.23	Ti, Fe
^{48}V	0.044	Ti, Fe
^{53}Mn	3.7×10^{6}	Fe
^{54}Mn	0.86	Fe
^{55}Fe	2.7	Fe
^{56}Co	0.215	Fe
^{59}Ni	8×10^{4}	Fe, Ni
^{60}Co	5.27	Co, Ni
^{81}Kr	2.1×10^{5}	Sr, Y, Zr

†^{10}Be, ^{36}Cl, ^{39}Ar, ^{46}Sc, and ^{60}Co are produced mainly by high energy galactic cosmic rays: ^{56}Co principally by solar cosmic radiation the remainder are produced by both type of cosmic rays.

Sources: Reedy, R. C. (1980) *Ancient Sun,* p. 370.
Lal, D. (1972) *Space Sci. Rev.* 14: 25.

Table 4.9b Some long-lived radionuclides, potentially useful in cosmic ray studies.

Radionuclide	Half-life (yr.)
^{42}Ar	33
^{44}Ti	47
^{63}Ni	100
^{32}Si	~300
^{91}Nb	~800
^{93}Mo	$\sim 3.5 \times 10^{3}$
^{94}Nb	2.0×10^{4}
^{41}Ca	1.3×10^{5}
^{233}U	1.6×10^{5}
^{60}Fe	$\sim 3 \times 10^{5}$
^{237}Np	2.1×10^{6}
^{129}I	1.6×10^{7}
^{236}U	2.3×10^{7}
^{92}Nb	3.3×10^{7}
^{146}Sm	1.0×10^{8}
^{40}K	1.28×10^{9}

Sources: Reedy, R. C. (1980) *Ancient Sun,* p. 370.
Lal, D. (1972) *Space Sci. Rev.* 14: 25.

lunar chronology. A very full discussion of the problems of interpretation of the irradiation record in this context is given by Burnett and Woolum [137].

4.10.1 Nuclear Track Data

Much information on exposure ages and regolith history has been obtained from the track studies. Track production at shallow depths (< 0.5 cm) is dominated by solar flares, while at greater depths, galactic cosmic ray tracks predominate [105, 106]. The "sun tan" exposure time is defined as the period during which a rock was at the surface of the Moon (usually less than 3 million years), while the "sub-decimeter" exposure time is the period during which a rock was within 10 cm of the surface (typically 1–100 million years).

High track densities, indicating surface exposure, are found throughout the core samples. The early interpretations were of a high rate of regolith turnover, but it quickly became clear that the regolith was stratified, and models involving deposition of thin layers, stirring of the surface, and burial by subsequent layers were adopted and so "throwout" models became preferred to "gardening" models [138]. This became clear from the study of the Apollo 15 deep core which contained forty-two strata, in which high track densities were distributed throughout the 242-cm core length and were independent of depth.

Many micron-sized particles with very high track densities have an amorphous surface layer from the solar bombardment. Each layer in the core contains grains throughout that were once at the "very surface," indicating good mixing of each layer before burial. Stirring takes place to a depth of a few centimeters. Deeper stirring is rare. Instead, overturning of layers by cratering occurs. Surface layers seem to survive for periods of from 1 to 50 million years before burial, as indicated by cratering studies (Section 4.3.2).

Exposure ages of rocks lying on the surface have been measured (Table 4.10). Most (80%) have a complex exposure history. Erosion by the micrometeorite bombardment and solar wind sputtering exposes fresh surfaces at rates of about one millimeter per million years.

Information about the exposure of old highland breccia fragments may be obtained from the track data, but this is offset by annealing due to heating during breccia formation. Because of this, the use of mare basalt rocks or individual grains in the regolith is preferred in cosmic ray studies. The tracks are largely inherited from the original parent materials which must have had exposure at the very top surface. Grains with track densities of $\geq 10^8/\text{cm}^2$ occur within the breccia matrix. The track densities correlate with metamorphic grade. Low track counts due to thermal annealing have occurred [139]. Tracks are absent in the well-recrystallized breccias (e.g., 15418, 61016, 66055, 67015) [140]. Tracks vanish first from the glasses during annealing, then

Table 4.10 Surface residence times for rocks apparently exposed in one orientation.

Rock	Mass (g)	Surface Residence Time (m.y.)
12018	787	1.7
12038	746	1.3
12022	1864	~10
62295	251	2.7
74275	1493	2.8
67915	*	50†
68815	*	2†
76315	*	21†

* Boulder chip.
† Surface residence time = total cosmic ray exposure time.
From Burnett, D. S., and Woolum, D. S. (1977) *PCE* 10: 87.

generally from olivine, pyroxenes, and feldspar in that order with increasing temperature.

There are a number of similarities between the lunar breccias and the gas-rich meteorites (e.g., Kapoeta, Fayetteville), which also contain grains exposed before incorporation in the meteorite with track densities of $\geq 10^{10}/cm^2$. Preserved solar flare tracks are seen even in the most recrystallized chondrites (e.g., LL6 grade [140, 141]), suggesting that even the most metamorphosed chondritic meteorites correspond only to the less metamorphosed lunar breccias [142]. The data seem consistent with the formation of the gas-rich meteorites in a regolith-type environment less extreme than that of the lunar surface, possibly on asteroid surfaces [140]. In this context, observations of the asteroid Toro suggest that it has a lunar-type regolith [143].

4.10.2 Rare Gas Data

The exposure history of the regolith and of surface rocks was one of the first applications of the rare gas studies. Of the various age methods, the most reliable are ^{81}Kr-^{83}Kr, ^{21}Ne, and ^{38}Ar ages [144]. The ^{3}He ages are subject to loss of He by diffusion. A full review of the data is provided by Burnett and Woolum [137] with appropriate cautionary tales.

The impact events dated by the ^{81}Kr technique are given in Table 4.11. The dating, of course, depends on the proper sampling of the ejecta blanket. Much confusion arose over the age of South Ray (Apollo 16), one of the freshest craters on the lunar surface. The ages of about 2 million years quoted in Table 4.11 are from rocks, and are in accord with the geological criteria [146]. Many of the soils, interpreted as South Ray ejecta, are far removed from the crater rim. South Ray is 640 m in diameter. The astronaut traverses came no closer than about 3 km, and fine ejecta from South Ray at about five

Table 4.11 Ages of lunar craters from ^{81}Kr studies.

	^{81}Kr Age (m.y.)	Reference*
Apollo 14: Cone Crater	25	1
Apollo 16: North Ray Crater	50	1
South Ray Crater	2.0	1
Apollo 17: Camelot Crater	90	2
Central cluster†	109	2
Shorty Crater	19	3

†If the central cluster of craters at Taurus-Littrow and the bright mantle landslide are due to secondaries from Tycho, this age provides a date for Tycho.

*References:

1. Burnett, D. S., and Woolum, D. S. (1977) *PCE* 10: 76.
2. Drozd, R. J., et al. (1977) *PLC 8:* 3027.
3. Eugster, O., et al. (1977) *PLC 8:* 3059.

crater diameters distant may not have been sampled [146]. Based on this interpretation, the astronauts sampled only scattered blocks from South Ray. A possible explanation is that most of the light-colored ejecta at this distance from the South Ray crater rim is derived from old thick regolith at the target site. Accordingly, it preserves an "older" age than that of the South Ray event (F. Hörz, pers. comm., 1981).

An equally interesting set of dates was obtained at the Apollo 17 site, where a site-wide event apparently occurred at about 100 million years ago [147]. This is equated with secondaries from Tycho, which accordingly provides one date for that event. The age of Camelot crater, thought to be older from photogeological evidence, is not distinguishable. A reevaluation of the photography has reconciled the data [148].

The exposure ages of regolith soils from the various missions typically show averages of about 400 million years with much spread in the data. Individual soil grains have been measured with ages up to 1.7 aeons [145]. In general, the exposure ages of rocks are complex, with ages ranging from 1 to 700 million years. A list of surface residence times of rocks which were apparently only exposed in one orientation is given in Table 4.10. The polymict brecciated chondrites, which may have originated in a young asteroidal regolith, have exposure ages less than about 50 million years [130].

4.11 Solar and Cosmic Ray History

The long-term stability of the sun is one of the fundamental scientific questions. Many locations on the lunar surface have not changed on a macroscale for 3 to 4 billion years, in great contrast to the terrestrial surface.

Accordingly, the lunar surface provides us with areas that have been exposed to solar radiation, although the record is complex in detail and complicated by little-understood problems, both within the sun, and on the lunar surface. Nevertheless, a useful amount of information is available and a picture is beginning to emerge of the history of the sun. A comprehensive account of the present state of knowledge is given in *The Ancient Sun: Fossil Record in the Earth, Moon and Meteorites* [149]. Although the detailed history of the sun lies outside the scope of this book, a synopsis of the present understanding, particularly as gathered from the lunar data, is useful. Superimposed on the short-term solar variability, perhaps best known through the 11- and 22-year cycles, are longer scale variations of which the best established is the Maunder Minimum period of reduced solar activity, when no sunspots, for example, were observed from about 1645 to 1715 A.D. [150].

The direct terrestrial record extends back several thousand years, using ^{14}C in trees, varves and ^{10}Be in polar ice [151–153]. However, the solar record in the lunar samples provides the possibility, in principle, of extending the record back to more than 4 billion years ago, within a few hundred million years of the formation of the sun. Comparative studies of microcraters and of solar flare tracks indicate that there is no convincing evidence for a change in the dust flux or the solar particle flux for the past 10^4–10^6 years. The long term Fe/H ratio is the same as the modern ratio [154] although some contrary opinions exist as to whether there was an episode of higher solar flare activity 2×10^4 years ago [155].

The solar flare and galactic cosmic ray fluxes in lunar samples and meteorites provide some very useful constraints on the history of the ancient sun [102]. Solar flare activity was present at least 4.2 aeons ago from the meteoritic record [156, 157]. The energy spectrum of the solar flare particles has not changed appreciably in the last 4 aeons. Thus, the track density profiles in ancient lunar and meteoritic samples is close to that recorded on a glass filter exposed at the Surveyor 3 site for three years (1967–70) and recovered during the Apollo 12 mission [158] (Fig 1.3). The enrichment of heavy particles in solar flares at low energies, relative to solar photosphere compositions, appears also in ancient flare records. There does not seem to be any good evidence for a higher incidence of solar activity during the early history of the Moon, as recorded in the lunar samples.

Evidence for the constancy of the galactic cosmic ray flux, composition of cosmic rays and of the energy spectrum may likewise be deduced from the track record, for the past 50 million years. The rare gas record [98] for the solar wind is similar for both present and ancient times, and the isotopic composition of Ar, Kr and Xe appear to have been invariant over the past 3–4 aeons [159]. This is in striking contrast to the record for nitrogen isotopic variations. The $^{15}N/^{14}N$ ratio has changed at a rate of 150 per mil per aeon for the past 2.5 aeons at least. This effect must reflect changes in the solar

photosphere or corona, since there is probably no indigenous nitrogen in the Moon (see Section 4.9.1). At present there is no theoretical explanation for this remarkable observation [118, 119].

Apart from this interesting fact, the overall impression is of relatively uniform solar conditions at least for 4 aeons. Unfortunately, there is not space here to discuss the interesting discrepancy between the geological evidence for the presence of liquid water on the surface of the Earth at 3.8 aeons [160] and theoretical models for solar evolution, which predict a solar luminosity of only about 70% of present day values [161]. Possibly, an early atmospheric greenhouse effect operated on the Earth if the astrophysical calculations are correct.

4.12 The Lunar Atmosphere

During the Apollo 17 mission, mass spectrometric measurements were made of the tenuous lunar atmosphere [162–165], which is, in fact, a collisionless gas. The primary components detected result from either the solar wind or from radioactive decay, and degassing of the spacecraft. Hydrogen, helium, neon and argon have been detected. The abundances are compatible with a solar wind source, except for ^{40}Ar, derived from radioactive decay of ^{40}K. During the lunar night, the temperature falls below 100° K, and the components from the degassing of the spacecraft mainly condense, thus allowing measurement of the indigenous components. Argon shows a predawn enhancement, consistent with the release of this condensible gas at the sunrise terminator. No components due to any volcanic activity have been detected and there is no evidence of any contribution to the present atmosphere from transient events, unless they are connected with degassing of ^{40}Ar.

A proposal of the existence of a lunar atmosphere 5×10^7 times the present atmosphere in the past 10^8 yr., deduced from the micrometeorite record [166], does not seem to be in accord with most of the other evidence [165].

4.13 Rare Gases and Planetary Atmospheres

The atmospheric compositions of Mars [167] and Venus [168, 169] have provided several surprises and important constraints on models of planetary evolution [131]. The rare or noble gases are separated into those produced at least partly by radiogenic decay (e.g., ^{4}He, ^{40}Ar, ^{129}Xe) and the primordial rare gases present in the solar nebula. Commonly measured isotopic species include ^{3}He, ^{4}He, ^{20}Ne, ^{36}Ar, ^{38}Ar, ^{84}Kr and ^{132}Xe. It is conventional to divide

Table 4.12 Rare gas contents of the atmospheres of Venus, Earth and Mars.

	^{36}Ar (Atmosphere) g/g	$^{40}Ar/^{36}Ar$	$^{20}Ne/^{22}Ne$	$^{20}Ne/^{36}Ar$
Venus	2.4×10^{-9}	1.0	14	0.3
Earth	3.5×10^{-11}	296	9.8	0.52
Mars	2.0×10^{-13}	3000	—	0.38
Solar Wind	—	< 1	13	28

the primordial rare gases into "solar" and " planetary." The "solar" rare gas composition is that derived from the sun via the solar wind. These abundances are well represented in the lunar soils (see Section 4.9.2). The "planetary" rare gas component is that observed in meteorites and is accordingly thought to represent the relative isotopic and elemental abundances in the solar nebula before accretion of the planets.

The rare gas compositions of the atmospheres of Venus and Mars given in Table 4.12 provide interesting new data. The principal results are that Venus has about 70 times the abundance of Ne and Ar observed in the terrestrial atmosphere, while Mars has much lower abundances than the Earth. These results are the reverse of what might have been expected from simple condensation models for planetary formation. The isotopic composition of neon in Venus, as shown by the $^{20}Ne/^{22}Ne$ ratios, is higher than that of the Earth, and is similar to the values observed in the solar wind. This indicates a differing source for neon in the Earth and Venus, once thought to be very similar planets. The abundance of ^{36}Ar in the Martian atmosphere is so low (about 180 times less than that of the Earth) that it is probably not due to a low rate of degassing. Evidence of this is given by the abundance of ^{40}Ar, derived from ^{40}K, in the Martian atmosphere. Mars probably has a low abundance of potassium (Table 8.5) and calculations based on $^{40}Ar/^{36}Ar$ ratios indicate that the bulk ^{36}Ar content of Mars is about an order of magnitude less than that of the Earth.

These data have caused us to revise our ideas on planetary evolution. There is not space here to discuss the many theories advanced to account for these data (see refs. [130] and [170–173]) but some tentative conclusions may be drawn. The high abundances of neon and argon in Venus may represent an early solar wind contribution to small planetesimals which accrete to form Venus. The low abundances of the planetary rare gases in Mars are likewise a primitive feature, due to the accretion of Mars from planetesimals depleted in neon, argon, krypton, and xenon. The new rare gas data lend support to the concept of planetary accretion of a heterogeneous collection of planetesimals (see Section 9.13).

4.14 Organic Geochemistry and Exobiology

A complete account of the organic geochemistry investigations on lunar samples was given previously [174]. Little further work has been done on this subject and the interested reader is referred to the previous summary.

The account of the search for life in the lunar samples is given in the same reference [174] and need not be repeated here. It should be noted that the absence of life on the Moon was in accordance with the prediction of C. Huyghens in 1757 that "the Moon has no air or atmosphere surrounding it as we have, [and I] cannot imagine how any plants or animals whose whole nourishment comes from fluid bodies, can thrive in a dry, waterless, parched soil" [175]. The search for life on Mars has been dealt with exhaustively in other references [176, 177] and will not be treated here. The effective absence of organic compounds at the parts per billion level in the Viking organic mass spectrometric experiment seems decisive [178]. This contrasts with the development of life on Earth [179].

References and Notes

1. Hood, L. L., and Schubert, G. (1980) *Science*. 208: 49.
2. Thompson, T. W., et al. (1974) *Moon*. 10: 87; (1981) *Icarus*. 46: 201; See also Pettengill, G. H. (1978) *Ann. Rev. Astron. Astrophys*. 16: 265 for an extended review of radar observations of planets and satellites. See also Schultz, P. H., and Mendell, W. (1978) *PLC 9*: 2857 for a discussion of orbital infrared observations.
3. Keihm, S. J., et al. (1973) *EPSL*. 19: 337; (1973) *PLC 4*: 2503; Strangway, D. W., and Olhoeft, G. R. (1977) *Phil. Trans. Roy. Soc*. A285: 441.
4. Olhoeft, G. R., et al. (1975) *PLC 6*: 3333.
5. See Tang, C. H., et al. (1977) *JGR*. 82: 4305 for surface electrical properties of Mars.
6. See Hess, S. L., et al. (1977) *JGR*. 82: 4559 for a description of Martian meteorology.
7. See Moore, H. J., et al. (1977) *JGR*. 82: 4497 for a description of Martian surface properties.
8. Saari, J. M. (1964) *Icarus*. 3: 161.
9. Mendell, W. W., and Low, F. J. (1970) *JGR*. 75: 3319.
10. Gold, T. (1971) *PLC 2*: 2675.
11. The extreme case is the presence of the layer of "light gray fines" (12033) at Apollo 12, a KREEP-rich layer of exotic origin.
12. The XRF experiment samples only the top few microns of the surface. The gamma-ray experiment looks somewhat deeper (10–20 cm). Adler, I., et al. (1973) *PLC 4*: 2783; Metzger, A. E., et al. (1973) *Science*. 179: 800.
13. McCoy, J. E., and Criswell, D. R. (1974) *PLC 5*: 2991.
14. Berg, O. E. (1978) *EPSL*. 39: 377.
15. Hörz, F. (1973) NASA SP 315, 7–24.
16. Gold, T. (1970) *Icarus*. 12: 360; (1971) *Apollo 14 PSR*, p. 239.
17. A major source of information on the lunar regolith is given in *The Moon* (1975), Vol. 13, p. 1–359, which contains the proceedings of a conference on the lunar regolith held

at the Lunar Science Institute, Houston, Texas, November 1974. See also an excellent review by Langevin, Y., and Arnold, J. R., (1977) *Ann. Rev. Earth Planet. Sci.* 5: 499. See also Regolith Conference Abstracts, LPI. Nov. 1981.
18. NASA SP 289 (1972) 5–23.
19. Cooper, M. R., et al. (1974) *Rev. Geophys. Space Phys.* 12: 291.
20. Peeples, W. J., et al. (1978) *JGR.* 83: 3459.
21. Freeman, F. J. (1981) USGS Prof. Paper 1048, Chap. F.
22. Eberhardt, P. (1973) *Moon.* 8: 104.
23. Houston, W. N., et al. (1974) *PLC 5*: 2361; Carrier, W. D., et al. (1973) *PLC 3*: 3213; Houston, W. N., et al., ibid., 3255; Mitchell, J. K., et al., ibid., 3235; Mitchell, J. K., et al. (1973) *PLC 4*: 2437.
24. Cherkasov, I. I., and Shvarev, V. V. (1975) *Lunar Soil Science* (Trans. N. Kaner), Keter Publishing House, Jerusalem, 170 pp.
25. Quaide, W., and Oberbeck, V. (1975) *Moon.* 13: 27.
26. Hörz, F. (1977) PCE 10: 3.
27. Nishiizumi, K., et al. (1979) *EPSL.* 44: 409.
28. Schmitt, R. A., and Laul, J. C. (1973) *Moon.* 8: 190.
29. Schonfeld, E., and Meyer, C. (1972) *PLC 3*: 1415.
30. Shoemaker, E. M., et al. (1971) *PLC 1*: 2399.
31. Wood, J. A., et al. (1970) *PLC 1*: 965.
32. Bhandari, N., et al. (1972) *PLC 3*: 2811.
33. Papanastassiou, D. A., and Wasserburg, G. J. (1970) *EPSL.* 8: 1, 269; (1971) *EPSL.* 11: 37, 12: 36; (1972) *EPSL.* 13: 368; 17: 52.
34. Cliff, R. A., et al. (1972) *JGR.* 77: 2007; Mark, R. K., et al. (1973) *PLC 4*: 1785; Murthy, V. R., et al. (1972) *PLC 3*: 1503.
35. Wetherill, G. W. (1971) *Science.* 173: 389.
36. The $^{87}Sr/^{86}Sr$ ratio of 0.69898 is the Basaltic Achondrite Best Initial (or BABI) ratio [33].
37. Nyquist, L. E., et al. (1973) *PLC 4*: 1839.
38. Schaal, R. B., and Hörz, F. (1980) *PLC 11*: 1679.
39. McKay, D. A., et al. (1970) *PLC 1*: 673.
40. Chao, E. C. T., et al. (1971) *JGR.* 75: 7445.
41. McKay, D. S., et al. (1972) *PLC 3*: 988.
42. McKay, D. S., et al. (1971) *PLC 2*: 755.
43. Taylor, G. J., et al. (1978) *PLC 9*: 1959.
44. Adams, J. B., and McCord, T. B. (1973) *PLC 4*: 163; Rhodes, J. M., et al. (1975) *PLC 6*: 2291.
45. Via, W. N., and Taylor, L. A. (1976) *PLC 7*: 393.
46. Papike, J. J. (1981) LPS XII: 805.
47. Stroube, W. B., et al. (1978) *Meteoritics.* 13: 201.
48. Taylor, S. R., and McLennan, S. M. (1979) *GCA.* 43: 1551.
49. Simonds, C. H., et al. (1978) *JGR.* 83: 2773.
50. Gooding, J. L., et al. (1980) *EPSL.* 50: 171.
51. Gooding, J. L., and Keil, K. (1981) *Meteoritics.* 16: 17.
52. Cloud, P. (1970) *PLC 1*: 1794.
53. Taylor, S. R. (1973) *Earth Sci. Rev.* 9: 101.
54. Roedder, E., and Weiblen, P. W. (1970) *PLC 1*: 801.
55. Glass, B. P. (1976) *PLC 7:* 679.
56. Glass, B. P., and Barlow, R. A. (1979) *Meteoritics.* 14: 55.
57. Mason, B. H. (1979) *Smith. Contrib. Earth Sci.* 22: 14.
58. Glass, B. P. (1972) *JGR.* 77: 7057; Frey, F. A. (1977) *EPSL.* 35: 43.

59. Shaw, H. F., and Wasserburg, G. J. (1981) LPS XII: 967.
60. Taylor, H. P., and Epstein, S. (1970) *PLC 1*: 613.
61. Schnetzler, C. C. (1970) *Meteoritics*. 5: 221.
62. O'Keefe, J. A. (1970) *Science*. 168: 1209.
63. Epstein, S., and Taylor, H. P. (1973) *PLC 4*: 1559.
64. Kozyrev, N. (1963) *Nature*. 198: 979.
65. Pike, R. J. (1980) USGS Prof. Paper 1046 C.
66. Chao, E. C. T., et al. (1962) *Science*. 135: 97; (1964) *GCA*. 28: 971.
67. Labotka, T. C., et al. (1980) *PLC 11*: 1285.
68. Laul, J. C., and Papike, J. J. (1980) *PLC 11*: 1307.
69. Rhodes, J. M. (1977) *Phil. Trans. Roy. Soc.* A285: 293.
70. Hörz, F. (1978) *PLC 9*: 3311.
71. Hubbard, N. J. (1979) *PLC 10*: 1753.
72. Laul, L. C., and Papike, J. J. (1980) *PLC 11*: 1307. It should be noted that both Ni and Co data reported in this study are probably contaminated through the use of rhodium plated nickel sieves.
73. Korotev, R. L., et al. (1980) *PLC 11*: 395.
74. Muehlberger, W. R., et al. (1980) *Lunar Highlands Crust*, p. 1.
75. Kempa, M. J., et al. (1980) *PLC 11*: 1341.
76. Heiken, G. (1975) *Rev. Geophys. Space Phys.* 13: 567.
77. Nagata, T., et al. (1974) *PLC 5*: 2815.
78. Cisowski, C. S., et al. (1974) *PLC 5*: 2841.
79. Chou, C. L., and Pearce, G. W. (1976) *PLC 7*: 779.
80. Morris, R. V. (1980) *PLC 11*: 1697.
81. Boynton, W. V., et al. (1976) *EPSL*. 29: 21.
82. Wëgmuller, F., et al. (1980) *PLC 11*: 1763.
83. Butler, P. (1978) *PLC 9*: 1459.
84. Cirlin, E. H., et al. (1978) *PLC 9*: 2049.
85. Cirlin, E. H., and Housley, R. M. (1979) *PLC 10*: 341; (1981) *PLC 12*: 529.
86. Gibson, E. K. (1977) PCE 10: 57.
87. Kurat, G., and Keil, K. (1972) *EPSL*. 14: 7.
88. Arnold, J. R. (1979) *JGR*. 84: 5659.
89. Fremlin, J. H. (1979) *Nature*. 278: 598.
90. Morgan, J. W., et al. (1977) NASA SP 370, 659.
91. Wasson, J. T., et al. (1975) *Moon*. 13: 121.
92. Schneider, E. (1973) *PLC 4*: 3277.
93. Hörz, F., et al. (1971) *JGR*. 76: 5770; Hartung, J. B., et al. (1973) *PLC 4*: 3213; Morrison, D. A., et al., ibid., 3235; Neukum, G., et al., ibid., 3255; Schneider, E., et al., ibid., 3277; Morrison, D. A., et al. (1972) *PLC 3*: 2767; Neukum, G., et al., ibid., 2793; Gault, D. E., et al., ibid., 2713; Hartung, J., et al., ibid., 2735; Hörz, F. (1975) *Planet. Space Sci.* 23: 151.
94. Frondel, C., et al. (1970) *PLC 1*: 445; Fredriksson, K., et al., ibid., 419.
95. Brownlee, D. E., et al. (1977) *PLC 8*: 149.
96. Hörz, F., et al. (1975) *PLC 5*: 2397.
97. Duennebier, F. K. (1976) *Science*. 192: 1000.
98. Borg, J. (1980) *Ancient Sun*, p. 431.
99. Pepin, R. O. (1980) *Ancient Sun*, p. 411.
100. Marti, K. (1980) *Ancient Sun*, p. 423.
101. Walker, R. M. (1975) *Ann. Rev. Earth Planet. Sci.* 3: 99.
102. Crozaz, G. (1977) PCE 10: 197.
103. Crozaz, G. (1980) *Ancient Sun*, p. 331.

104. Macdougall, J. D., et al. (1974) *Science*. 183: 73.
105. Price, R. B., Fleisher, R. L., and Walker, R. M. (1975) *Nuclear Tracks*, Univ. Calif. Press.
106. Lal, D. (1972) *Space Sci. Rev*. 14: 45.
107. Herrman, G. (1979) *Nature*. 280: 543.
108. Phakey, P. P., et al. (1972) *PLC 3*: 2905.
109. Crozaz, G., et al. (1972) *PLC 3*: 1623.
110. Crozaz, G. (1980) *Ancient Sun*, p. 311.
111. Epstein, S., and Taylor, H. P. (1970) *PLC 1*: 1085.
112. Eglinton, G., et al. (1974) *Topics in Current Chemistry*. 44: 88.
113. Pillinger, C. T. (1979) PCE 11: 61.
114. Becker, R. H., and Clayton, R. N. (1975) *PLC 6*: 2131.
115. Becker, R. H., et al. (1977) *PLC 8*: 3685.
116. Gibson, E. K. (1977) PCE 10: 57.
117. Muller, O. (1979) PCE 11: 47.
118. Clayton, R. N., and Thiemens, N. H. (1980) *Ancient Sun*, p. 463.
119. Kerridge, J. F. (1980) *Ancient Sun*, p. 475.
120. Goel, P. S., et al. (1975) *GCA*. 39: 1347.
121. Kerridge, J. F., et al. (1975) *PLC 6*: 2151.
122. Thode, H. G., and Rees, C. E. (1979) *PLC 10*: 1629.
123. Heymann, D. (1977) PCE 10: 45.
124. Heymann, D., and Yaniv, A. (1970) *PLC 1*: 1261.
125. Eberhardt, P., et al. (1970) *PLC 1*: 1037.
126. Baur, H., et al. (1972) *PLC 3*: 1947.
127. Signer, P., et al. (1977) *Phil. Trans. Roy. Soc.* A285: 385.
128. Yaniv, A., and Heymann, D. (1972) *PLC 3*: 1967.
129. Schultz, L. (1979) PCE 11: 39.
130. McElroy, M. B., and Prather, M. J. (1981) *Nature*. 293: 535. This article contains a review of the noble gases in the terrestrial planets.
131. Reedy, R. C. (1980) *Ancient Sun*, p. 370.
132. Wahlen, M., et al. (1972) *PLC 3*: 1719.
133. Reedy, R. C., and Arnold, J. R. (1972) *JGR*. 77: 537.
134. Fields, P. R., et al. (1973) *PLC 4*: 2123.
135. Burnett, D. S., and Woolum, D. S. (1974) *PLC 5*: 2061.
136. Russ, G. P. (1973) *EPSL*. 16: 275.
137. Burnett, D. S., and Woolum, D. S. (1977) PCE 10: 63.
138. Arrhenius, G., et al. (1971) *PLC 2*: 2583.
139. Hart, H. R., et al. (1972) *PLC 3*: 2831; Hutcheon, I. D., et al., ibid., 2845, 2863; Dran, J. C., et al. (1972) *PLC 3*: 2883; Yuhas, D. E., et al. (1972) *PLC 3*: 2941.
140. Macdougall, J. D., et al. (1973) *PLC 4*: 2319.
141. Van Schmus, W. R., and Wood, J. A. (1967) *GCA*. 31: 747.
142. Crozaz, G., et al. (1974) *PLC 5*: 2475.
143. Dunlap, J. L., et al. (1973) *Astron. J*. 78: 491.
144. Marti, K. (1967) *Phys. Rev. Lett*. 18: 264; Lugmair, G. W., and Marti, K. (1972) *PLC 3*: 1891; Marti, K., et al. (1973) *PLC 4*: 2037.
145. Kirsten, T., et al. (1972) *PLC 3*: 1865.
146. McKay, D. S., and Heiken, G. H. (1973) *PLC 4*: 41.
147. Drozd, R. J., et al. (1977) *PLC 8*: 3027.
148. Lucchitta, B. K. (1979) *Icarus*. 37: 46.
149. *The Ancient Sun: Fossil Record in the Earth, Moon and Meteorites* (1980) (eds., Pepin, R. O., et al.), Pergamon, 581 pp.

150. Those readers with a historical bent will reflect on the curious fact that the Maunder Minimum of solar activity 1645–1715, coincided with the life of the Sun King (Louis XIV, 1638–1715), a correlation no doubt of use to Francophiles and Francophobes alike.
151. Stuiver, M., and Grootes, P. M. (1980) *Ancient Sun*, p. 165.
152. Fairhill, A. W., and Yorg, I. C. (1980) *Ancient Sun*, p. 175.
153. Raisbeck, G. M., and Yiou, F. (1980) *Ancient Sun*, p. 185.
154. Zinner, E. (1980) *Ancient Sun*, p. 201.
155. Zook, H. A. (1980) *Ancient Sun*, p. 245.
156. Macdougall, J. D., and Kothari, B. K. (1976) *EPSL*. 33: 36.
157. Goswami, J. N. (1980) *Ancient Sun*, p. 347.
158. Crozaz, G., and Walker, R. M. (1971) *Science*. 171: 1237.
159. Marti, K. (1980) *Ancient Sun*, p. 423.
160. Windley, B. F. (1977) *The Evolving Continents*, Wiley.
161. Newkirk, G. (1980) *Ancient Sun*, p. 293.
162. NASA SP-330.
163. Hodges, R. R., et al. (1973) *PLC 4*: 2854; (1974) *Icarus*. 21: 415.
164. Hoffman, J. H., et al. (1973) *PLC 4*: 2865.
165. Hodges, R. R., et al. (1974) *Icarus*. 21: 415 gives a comprehensive review of the lunar atmosphere.
166. Chernyak, Y. B. (1978) *Nature*. 273: 497.
167. McElroy, M. B., et al. (1977) *JGR*. 82: 4379.
168. Hoffman, J. H., et al. (1980) *JGR*. 85: 7882.
169. Donahue, T. M., et al. (1981) *GRL*. In press.
170. Anders, E., and Owen, T. (1977) *Science*. 198: 453.
171. Pollack, J. B., and Black, D. C. (1979) *Science*. 205: 56; Pollack, J. B., and Yung, Y. L. (1980) *Ann Rev. Earth Planet. Sci*. 8: 425.
172. Wetherill, G. W. (1981) *Icarus*. In press.
173. Hostetler, C. J. (1981) *PLC 12*: 1387.
174. Taylor, S. R. (1975) *Lunar Science: A Post-Apollo View*, Pergamon, N.Y., p. 110–114.
175. Huyghens, C. (1757) *Cosmotheoros*.
176. The biological experiments are described in (1977) *JGR*. 82: 4659–4677.
177. An extended and readable account is given by H. S. F. Cooper (1980) in *The Search for Life on Mars*, Dial Books.
178. Biemann, K., et al. (1977) *JGR*. 82: 4641.
179. Schopf, J. W., ed. (1982) *Origin and Evolution of the Earth's Earliest Biosphere*, Princeton Univ. Press.